Leading Our World In Motion

2005-01-3837

SAE TECHNICAL
PAPER SERIES

The Influence of Charge Dilution and Injection Timing on Low-Temperature Diesel Combustion and Emissions

Sanghoon Kook and Choongsik Bae
Korea Advanced Institute of Science and Technology

Paul C. Miles, Dae Choi and Lyle M. Pickett
Sandia National Laboratories

**Powertrain & Fluid Systems
Conference and Exhibition
San Antonio, Texas USA
October 24-27, 2005**

SAE International™

400 Commonwealth Drive, Warrendale, PA 15096-0001 U.S.A. Tel: (724) 776-4841 Fax: (724) 776-5760 Web: www.sae.org

All SAE papers, standards, and selected books are abstracted and indexed in the Global Mobility Database.

ISSN 0148-7191

2005-01-3837

The Influence of Charge Dilution and Injection Timing on Low-Temperature Diesel Combustion and Emissions

Sanghoon Kook and Choongsik Bae
Korea Advanced Institute of Science and Technology

Paul C. Miles, Dae Choi and Lyle M. Pickett
Sandia National Laboratories

ABSTRACT

The effects of charge dilution on low-temperature diesel combustion and emissions were investigated in a small-bore single-cylinder diesel engine over a wide range of injection timing. The fresh air was diluted with additional N_2 and CO_2, simulating 0 to 65% exhaust gas recirculation in an engine. Diluting the intake charge lowers the flame temperature T due to the reactant being replaced by inert gases with increased heat capacity. In addition, charge dilution is anticipated to influence the local charge equivalence ratio ϕ prior to ignition due to the lower O_2 concentration and longer ignition delay periods. By influencing both ϕ and T, charge dilution impacts the path representing the progress of the combustion process in the ϕ-T plane, and offers the potential of avoiding both soot and NO_x formation.

In-cylinder pressure measurements, exhaust-gas emissions, and imaging of combustion luminosity were performed to clarify the path of the combustion process and the effects of charge dilution and injection timing on combustion and fuel conversion efficiency. Based on the findings, a postulated combustion process in the ϕ-T plane is presented for different dilution levels and injection timings. Although the ignition delay increased with high dilution and early injection, the heat release analysis indicated that a large portion of the combustion and emissions formation processes was still dominated by the mixing-controlled phase rather than the premixed phase. Because of the incomplete premixing, and the need to mix a greater volume of charge with unburned or partially-burned fuel to complete combustion, the diluted mixtures increased CO emissions. Injecting the fuel at earlier timings to extend the ignition delay helped alleviate this problem, but did not eliminate it. Fuel conversion efficiencies calculated for each dilution level and start of injection provide guidance as to the appropriate combustion phasing and practical levels of charge dilution for this low-temperature diesel combustion regime.

INTRODUCTION

Low-temperature diesel combustion systems limit combustion temperatures to levels at which NO_x and soot formation rates are low. These systems can be roughly divided into two categories: those in which the combustion phasing is largely decoupled from injection timing and dominated by the kinetics of the chemical reactions, and those in which the control of the combustion phasing is closely coupled to the fuel injection event. In the former category, the fuel and air are typically thoroughly premixed, such that at the start of combustion the mixture is near homogeneous and characterized by an equivalence ratio ϕ that is everywhere less than 1. Such systems are generally termed homogeneous charge compression ignition (HCCI) systems. Low combustion temperatures are achieved by either pre-mixing to very lean equivalence ratios ($\phi \leq 0.5$) or by employing exhaust gas recirculation (EGR) to reduce the combustion temperatures of mixtures with higher equivalence ratio (and to control the combustion phasing, *e.g.* [1, 2]).

In contrast, for the second category, the short times between the fuel injection event and the start of combustion preclude thorough pre-mixing, and significant regions exist where $\phi > 1$ at the start of combustion. Accordingly, a large fraction of the heat is released in a mixing-controlled process and peak combustion temperatures near the adiabatic flame temperature of a stoichiometric mixture could be realized. Various strategies are used to keep the flame temperatures low, including low compression ratio, large amounts of cooled EGR, and use of retarded injection timing. This latter category of low-temperature combustion systems is the focus of this paper.

Charge dilution through use of EGR is a widely used strategy employed for maintaining low flame temperatures and low NO_x emissions in diesel engines [3, 4]. Soot emissions are typically found to increase with

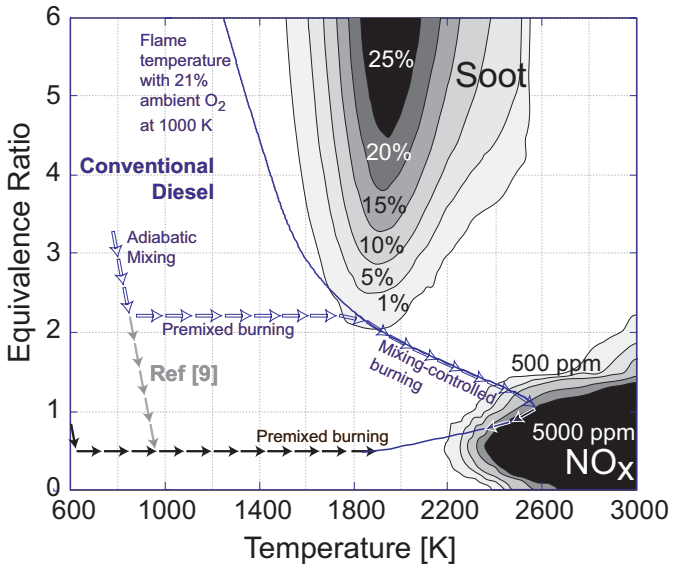

Fig. 1 Depiction of conventional and two variants of low-temperature combustion on the ϕ-T plane

increasing dilution, however. Soot emissions from diesel engines are a result of a competition between soot formation and oxidation processes. Traditionally, it has been thought that charge dilution affects the oxidation processes more strongly, and soot emissions increase due to a reduction in oxidation rates associated with the low flame temperatures of dilute mixtures. A recent study [6], however, suggests that low soot formation rates may also be achievable with very high levels of charge dilution, as the flame temperature is limited to levels at which the soot formation rate is low.

Understanding of the soot and NO_x formation processes can be aided through examination of the combustion process in a ϕ-T parameter space [7], which has proven to be a useful tool for visualizing how the combustion and emission formation/destruction processes progress.

An example is shown in Fig. 1. The figure is an equivalence ratio versus temperature plot with contours indicating the locations where soot and NO_x formation occur for a diesel-like fuel. Here, the zones of soot and NO_x formation are sketched according to the numerical results of Kitamura *et al.* [8], for *n*-heptane fuel at a pressure of 6 MPa and a residence time of 2 ms. Also a solid line shown in the figure is the maximum flame temperature achieved for fuel at 373 K reacting with ambient gas at temperature of 1000 K. The open arrows are the path followed by a typical fuel element in the ϕ-T plane for a conventional diesel combustion process.

Injection of fuel into the combustion chamber initiates an adiabatic mixing process which, after the ignition delay, is followed by rapid heat release that brings the mixture to the flame temperature. During this premixed burning process, the heat release is rapid and little additional mixing takes place. Subsequently, additional mixing with oxidant or with the products of more complete combustion causes the path of the fuel element to follow the flame temperature curve. Beyond ϕ = 1, no significant chemical heat release occurs and mixing serves to lower the temperature of the fuel element.

Two additional, contrasting paths are also shown on Fig. 1. The first, denoted by the black arrows, depicts a typical HCCI combustion process, in which mixing is substantially complete before the onset of combustion. The second path, denoted by the gray arrows, is the path one might expect to follow if complete mixing to a lean equivalence ratio is achieved even after the time of premixed burn, made possible by high rates of mixing before the lift-off length using small injector holes and high injection pressures [9]. Note that these latter paths are expected to produce very little soot or NO_x emissions.

It is evident from the above description that the formation of both soot and NO_x depends strongly on the path followed during the combustion process. A major objective of this study is thus to clarify the effect of EGR rate and start of injection (SOI) on the path of a diesel combustion process. The EGR rate influences the path not only through changes in the flame temperature, but also in ignition delay and the amount of ambient fluid that must be mixed with the fuel to attain a given equivalence ratio. Similarly, the SOI influences the temperature (and density) during the ignition delay period, the peak flame temperature reached, and the cooling of the in-cylinder charge during the latter part of the combustion process as volume expansion takes place.

In previous work [10], we have begun to clarify the path followed for a subset of low-temperature combustion systems characterized by moderate EGR rates and retarded injection timings (examples of these systems include “MK (Modulated Kinetics)” combustion [11], “HCLI (Homogeneous Charge Late Injection)”, and “HPLI (Highly Premixed Late Injection)” combustion [12]). Here, we vary both the EGR rate and start of injection over a broad range encompassing not only the aforementioned combustion systems, but also conventional diesel combustion and early injection systems such as the Toyota “smokeless” system [6] or the “DCCS (Dilution Controlled Combustion System)” [12].

Subsequently, we contrast the various parameters influencing the ϕ-T plane path of the combustion process, the emission formation/destruction rates along the path, and (qualitatively) sketch the path itself. The various factors influencing the fuel conversion efficiency of these combustion systems are also considered.

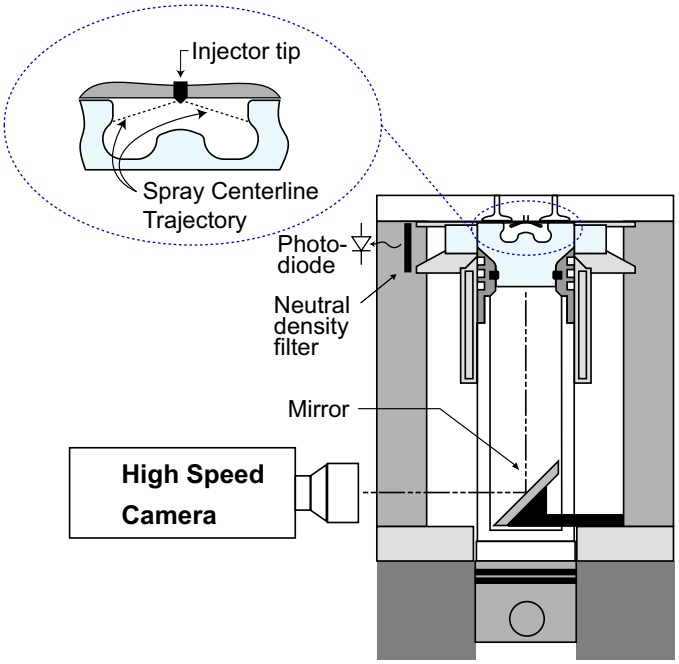

Fig. 2 Optical single-cylinder diesel engine

Table 1 Engine specifications

Basic Geometry

Bore: 79.5 [mm]	Stroke: 85.0 [mm]
Disp. Vol.: 422 [cm^3]	Comp. Ratio: 18.7

Valve Events

IVO: -360 CAD ATC	EVO: 145 CAD ATC
IVC: -140 CAD ATC	EVC: -350 CAD ATC

Fuel Injection Equipment

Bosch Flow No.: 320	Included Angle: 145˚
Number of Holes: 6	Hydro-erosion: 10 %
Nozzle Style: Cylindrical Minisac (Bosch DLLA)	

Table 2 Operating Parameters

Speed [rpm]	1500
$T_{Coolant}$ [˚C]	88
$P_{Injection}$ [bar]	800
Swirl Ratio [R_s]	3.77
P_{Intake} [bar]	1.2
T_{Intake} [˚C]	90
$P_{Exhaust}$ [bar]	1.3
Start Of Injection (SOI) [CAD ATDC]	-30.25 to 7.75

EXPERIMENT

RESEARCH ENGINE & DIAGNOSTICS

Measurements were obtained in a single-cylinder optical diesel engine with typical characteristics of small-bore engines intended for automotive applications, *i.e.*: four valves, a central, vertical injector, 6-hole minisac nozzle, and a concentric, re-entrant bowl. A schematic of the engine is shown in Fig. 2, and its specifications are shown in Table 1. Fuel injection parameters—including injection pressure, injected mass and injection timing—were controlled with a common-rail fuel system, capable of a maximum injection pressure of 1350 bar.

In-cylinder pressure was acquired using a water-cooled (KISTLER 6043A60) piezoelectric pressure transducer. The in-cylinder pressures acquired over 50 engine cycles were averaged to calculate the indicated mean effective pressure (IMEP), the apparent heat release rate, and the cumulative heat release. In-cylinder pressure data, and the photodiode luminosity data described below, were acquired with a resolution of 0.25 crank angle degrees (CAD).

Engine-out NO_x was measured using a California Analytical Instruments chemiluminescent NO_x analyzer (Model 600-HCLD). Samples were taken from the exhaust plenum and transferred to the analyzer through a heated sample line. Moisture and condensable hydrocarbons were removed from the sample by a condenser prior to the analyzer. Samples were also analyzed for CO content using a California Analytical Instruments NDIR (Non-Dispersive Infra-Red) CO analyzer (Model 300).

The formation and spatial distribution of in-cylinder soot was monitored with two optical diagnostics. First, a spatially-integrated measure of natural combustion luminosity was obtained with a high-sensitivity photodiode viewing the combustion chamber through the liner window. Because the luminosity from hot soot is considerably stronger than the luminosity from natural chemiluminescence [14], the photodiode data is dominated by soot luminosity at all but the highest EGR rates and extremes of injection timing. Neutral density filters were selected to maintain the signal level within the range of the photodiode signal saturation.

Second, images of natural combustion luminosity were obtained to provide qualitative information on the spatial distribution of luminous soot within the combustion chamber. Both bottom-view images acquired through the extended piston assembly (as illustrated in Fig. 2) and side-view images acquired through the liner side windows were obtained. A high speed digital video camera (Integrated Design Tools Inc.; X-Stream Vision) was employed to obtain these images. The frame rate was set to 9000 frames per second, corresponding to 1 CAD (Crank Angle Degree) at 1,500 rpm. The image resolution is 280 x 280 pixels and an exposure time of 30 μs (0.297 CAD) was employed.

ENGINE OPERATION

The engine operating parameters are described in Table 2. All data were acquired at a fixed engine speed of 1500 rpm. The coolant temperature was set to 88˚C.

Recirculated exhaust gas was simulated by diluting the intake air stream with N_2 and CO_2. The proportions of air, CO_2, N_2 were selected to obtain the desired O_2 concentration. The relative proportions of CO_2 and N_2 were chosen to match the mixture molar specific heat of real engine exhaust gas at the selected load and O_2 concentration. The selected O_2 concentrations, the corresponding EGR rates, stoichiometric air-fuel ratio, and the calculated average in-cylinder equivalence ratios are listed in Table 3.

Prior to obtaining in-cylinder pressure and exhaust emissions, the engine was motored for a minimum of 90 s in order to pre-heat the combustion chamber walls and to allow the intake plenum pressure to stabilize. Subsequently, the engine was skip-fired for 70 s, with fuel injection occurring on only one of every four engine cycles. This skip-firing period allowed the emission analyzers to stabilize. Finally, data were acquired over 50 additional skip-fired cycles for the pressure, emissions, and spatially-integrated luminosity data. For imaging of the spatial distribution of soot luminosity, or acquisition of spatially-integrated luminosity at high O_2 concentration (19 and 21%), window fouling considerations dictate that the data be acquired immediately upon starting skip-fired operation. Accordingly, before acquiring these data, the engine was motored for an extended period to raise cylinder wall temperatures to levels commensurate with those existing after the 70 s skip-firing period.

Table 3 Charge Dilution

O_2 [%]	N_2 [%]	CO_2 [%]	EGR [%]	$(A/F)_{st}$	Avg. ϕ
21.0	79.0	0.0	00.0	14.5	0.266
19.0	79.3	1.7	25.0	16.1	0.295
17.1	79.6	3.3	40.0	18.1	0.330
15.1	79.8	5.0	50.0	20.6	0.375
13.8	80.0	6.1	55.0	22.7	0.412
12.2	80.3	7.5	60.0	25.9	0.470
11.2	80.4	8.4	62.5	28.3	0.512
10.1	80.6	9.3	65.0	31.6	0.570

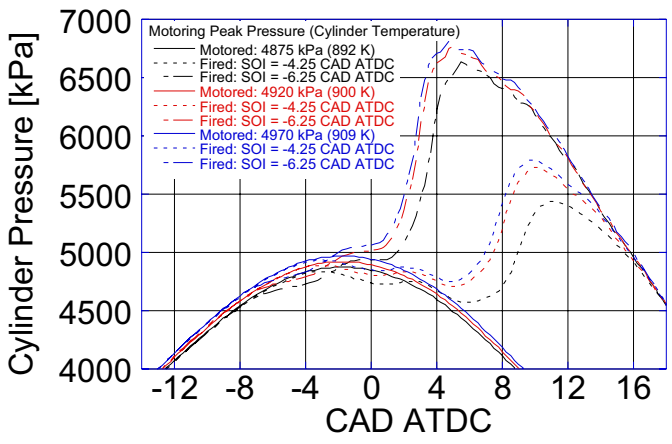

Fig. 3 Change of combustion phasing with different peak motoring pressure (bulk temperature)

While performing injection timing sweeps, the in-cylinder density was fixed by maintaining a fixed intake mass flow rate. Accordingly, to maintain the same average in-cylinder temperature ("bulk" temperature) for all tests, the same in-cylinder pressure history must be attained. With changing SOI, this pressure history varies slightly, for reasons thought to be associated with changes in the cylinder wall temperatures. Therefore, for some tests, the motored period was extended from the minimum of 90 s to match the motored pressure traces before the injection event. Figure 3 shows how changes in the bulk temperature, manifested as small changes in the pressure trace before injection, can cause significant differences in firing pressure traces and combustion phasing. The in-cylinder pressure data obtained is repeatable to within ±10 kPa, corresponding to a bulk in-cylinder temperature tolerance of approximately ±2 K.

For the EGR sweeps (fixed SOI), the pressure traces before injection were also carefully controlled to match the bulk in-cylinder temperature as shown in Fig. 4. This was accomplished by fixing the total intake mass flow rate at all EGR rates, such that the bulk gas density remained fixed, and by adjusting the motored period so that the in-cylinder pressure decreases as much as the gas constant R decreases for diluted gases ($Pv = RT$). Following this procedure, slightly lower TDC pressures are observed as the EGR rate is increased.

The fueling rate was controlled to maintain 3 bar IMEP (indicated mean effective pressure) for different SOI and EGR cases. If the fueling rate was over ± 10 % of the reference case, the SOI and EGR sweeps were stopped. The reference was 7.7 mg/stroke injected for 21 % O_2 concentration and SOI of -4.25 CAD ATDC.

DATA ANALYSIS

HEAT RELEASE ANALYSIS

The in-cylinder pressure data were analyzed for the apparent heat release rate using an iterative, two-zone heat release code, in which gas properties are dependent on both mixture composition and temperature. The heat transfer losses are partially accounted by subtracting the apparent heat release calculated for a corresponding motored engine cycle, a procedure which is also expected to compensate to a large degree for enthalpy losses associated with crevice flows.

Consequently, the net apparent heat release rate $\dot{Q}_{app}$ is approximately equal to the rate of chemical heat release $\dot{Q}_{chem}$ less the difference between the heat transfer losses $\dot{Q}_{hl}$ with combustion $\dot{Q}_{ht,comb}$ and the motored losses $\dot{Q}_{ht,motored}$:

$$\dot{Q}_{app} = \dot{Q}_{chem} - \left(\dot{Q}_{ht,comb} - \dot{Q}_{ht,motored}\right) = \dot{Q}_{chem} - \dot{Q}_{hl} \qquad (1)$$

The cumulative apparent heat release history is obtained by integrating $\dot{Q}_{app}$ from SOI until the integral reaches a maximum Q_{total} just prior to exhaust valve opening. Normalized (fractional) heat release histories are calculated by normalizing the cumulative heat release by Q_{total} . These normalized histories are used to determine burn periods and to estimate equivalence ratios at ignition, as described below.

ADIABATIC FLAME TEMPERATURE

To clarify the effects of flame temperature on the combustion process and engine emissions, several parameters are correlated below with the maximum adiabatic flame temperature T_f . This methodology has been proven as a reasonable approach to analyze engine-out emissions by Plee *et al.* [3] and Musculus [5] as well. The adiabatic flame temperature was calculated for a stoichiometric mixture of diesel fuel and diluted intake gas using the STANJAN chemical equilibrium code [15]. The peak adiabatic flame temperature is here defined as the adiabatic flame temperature achieved by combustion of a stoichiometric mixture at the peak gas temperature ("core" temperature). The peak gas temperatures were estimated from the initial intake gas temperature and pressure assuming that the core gases are compressed isentropically. The estimation accounted for the gas composition and for temperature dependent specific heats. For the flame temperature calculation, a single heat of combustion was used for the multi-component diesel fuel, calculated from the net heat of combustion and H/C ratio as given in Table 4.

RESULTS AND DISCUSSION

IN-CYLINDER PRESSURE

At fixed SOI, charge dilution decreases the peak in-cylinder pressure due to the higher heat capacity of the diluent gases as well as slower reaction rates during the premixed combustion. Figure 4 shows the variation in the in-cylinder pressure traces for the various inlet gas O_2 concentrations at a fixed injection timing of -6.25 CAD ATDC.

Despite the above–mentioned reduction in peak pressure at fixed SOI, the highest in-cylinder pressures are often observed at the lower O_2 concentration. Under these circumstances, the long ignition delay and slow premixed combustion permitted very advanced injection timing. As a result, the portion of fuel burned during the latter part of the compression stroke increased, and the peak in-cylinder pressure increased when the timing is advanced, as shown in Fig. 5.

Table 4 Fuel Properties

2007 Emission Certification Diesel Fuel	
Cetane Number	47.1
H/C Ratio	1.825
Net Heat of Combustion	42.98 [kJ/kg]
Specific Gravity	0.8406
Viscosity at 40 ˚C	2.2
Flash Point	77 [˚C]
Particulate Matter	11.6 [mg/l]
Sulfur	8.1 [ppm]
Carbon wt%	86.72
Hydrogen, wt%	13.28

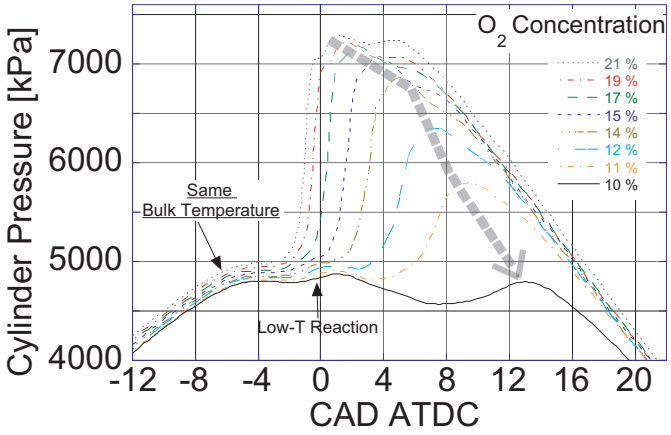

Fig. 4 Effect of charge dilution on cylinder pressure (SOI= -6.25 CAD ATDC)

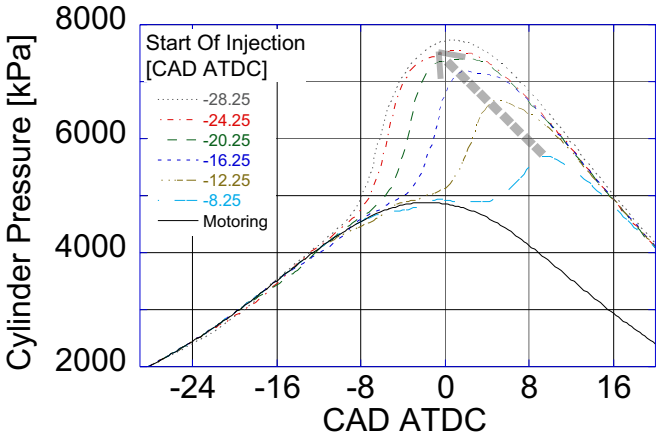

Fig. 5 Effect of injection timing on cylinder pressure (10% O_2 concentration)

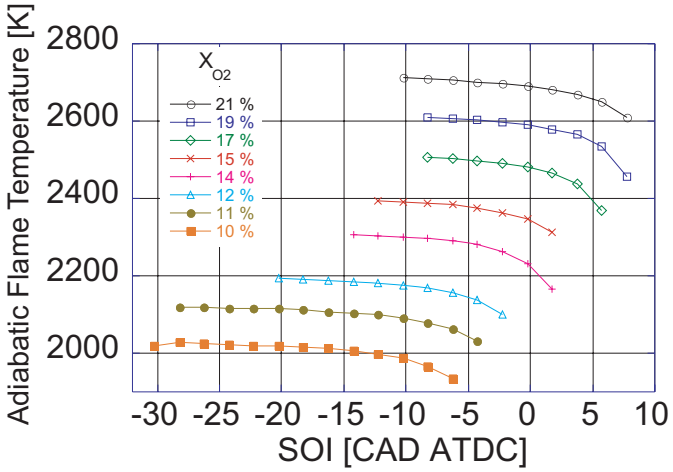

Fig. 6 Peak adiabatic flame temperature for a stoichiometric flame

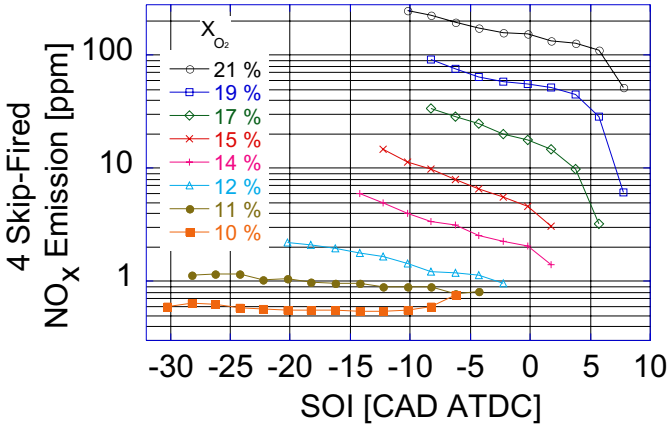

Fig. 7 Effect of O_2 concentration and injection timing on NO_x emission

ADIABATIC FLAME TEMPERATURE

The peak adiabatic flame temperature calculated for each EGR rate and SOI is shown in Fig. 6. Because the peak adiabatic flame temperature is based on the peak in-cylinder temperature, the additional compression associated with early heat release, discussed in conjunction with Fig. 5, generally results in an increase in adiabatic flame temperature as SOI is advanced at any fixed O_2 concentration. This behavior can be clearly seen in Fig. 6. Although the peak pressures for low O_2 concentration are often higher than those seen at greater O_2 concentrations due to the advanced injection timing, overall the peak adiabatic flame temperatures are lower. More specifically, at fixed SOI the peak flame temperature is always observed to decrease with decreasing O_2 concentration.

NO_x EMISSIONS

The NO_x emissions measured for an injection timing sweep at each of the eight O_2 concentrations are shown in Fig. 7. As noted in the Experiment section, emissions were measured operating the engine in a skip-fired mode. Had the engine been continuously fired, the emissions would be 4 times the value shown. Figure 7 indicates that, for all but the lowest O_2 concentration, NO_x emissions are reduced as injection timing is retarded. Also note that, at fixed injection timing, NO_x decreases with decreasing O_2 concentration—behavior which is consistent with the calculated maximum flame temperatures shown in Fig. 6.

From the extended Zeldovich mechanism of NO formation, adopting a partial equilibrium assumption [16], an approximate NO formation rate can be written as

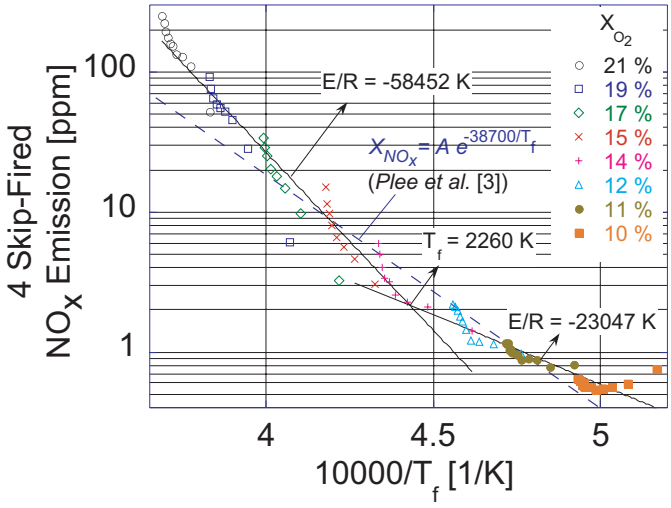

Fig. 8 Correlation of NO_x emission with the stoichiometric flame temperature, obtained with reactants initially at the maximum gas temperature ("core" temperature)

$$\frac{d}{dt}[NO] = A\,T^{-1/2}[O_2]^{1/2}[N_2]e^{E_a/RT}\ mol/cm^3 \cdot s \qquad (2)$$

where A is a constant, T is the local gas temperature, R is the universal gas constant, and E_a is an overall activation energy.

Figure 8 illustrates the flame temperature correlation obtained when NO_x emissions are plotted against T_f^{-1} on a semi-log plot. Plee *et al.* [3] suggest that the effect of charge dilution on NO_x emissions is primarily due to a lowering of flame temperature, and that the exhaust gas NO_x mole fraction can be correlated with an expression similar to Eq.(2):

$$X_{NO_x} = A \cdot e^{E_a/RT_f} \qquad (3)$$

where T_f is the stoichiometric adiabatic flame temperature. The theoretical basis for Eq.(3) is the premise that engine-out NO_x emissions will be proportional to the peak NO_x formation rate. Plee *et al.* obtain $E_a/R = -38700\ K$ from their experimental data. NO_x emissions are thus decreased exponentially with decreasing flame temperature.

Figure 8 indicates that only a partial correlation of the NO_x emissions measured here with peak flame temperature is obtained using Eq.(3). Two significant deviations are observed. First, the slope of the correlation (activation energy E_a/R) decreases in magnitude at lower temperatures (higher T_f^{-1}). Second, the activation energies obtained differ from the value obtained by Plee and co-workers.

In the first region, where $T_f > 2260\ K$, the data are well correlated by

$$X_{NO_x} = 3.77\times10^{11} \cdot e^{E_a/RT_f} \qquad (4)$$

where $E_a/R = -58452\ K$.

In the second, low-temperature region ($T_f < 2260\ K$), the apparent activation energy is decreased in magnitude and the correlation is better expressed as:

$$X_{NO_x} = 5.92\times10^{4} \cdot e^{E_a/RT_f} \qquad (5)$$

with $E_a/R = -23047\ K$.

The two regions of the NO_x correlation with flame temperature have also been observed by Plee *et al.*, although their low-temperature measurements were not as extensive as is seen in Fig. 8 due to the higher O_2 concentrations considered. The cause of the different behavior in the low-temperature region has not yet been identified, but several possibilities exist:

1. Because NO_x emissions are lower than 2 ppm (8 ppm had the engine been continuously fired), it is possible that flame temperatures are low enough that thermal NO formation no longer dominates, and "prompt" NO formation becomes significant [3].

2. Due to the low temperatures, formation reactions may be quenched earlier [3].

3. At the lowest O_2 concentrations, less fuel may be found in stoichiometric or leaner mixtures prior to ignition, and the peak flame temperature for the remaining, rich fuel mixtures is not reached until later in the cycle, after additional mixing has taken place. By this time, cylinder volume expansion has cooled the gases. Estimates of the equivalence ratio at ignition and a simple adiabatic mixing analysis presented below support this suggestion.

Regardless of the cause, the trends observed in Figs. 7 and 8 are clear: at the lowest O_2 concentrations NO_x emissions are less sensitive to SOI despite the significant variation in calculated peak flame temperature (Fig. 6).

Although NO_x emissions correlate reasonably well with peak adiabatic flame temperature alone, examination of Eq.(2) suggests that NO_x emissions might be affected by other, additional parameters. That is, for the constant density tests conducted here,

$$X_{NO_x} \propto X_{O_2}^{1/2} X_{N_2} M^{-1/2} T_f^{-1/2} \cdot e^{E_a/RT_f} \qquad (6)$$

For various O_2 concentrations, both the mixture molecular weight M and the N_2 mole fraction X_{N_2} vary little (from 28.96 to 29.95 and from 79 to 80.6 (see Table 3), respectively). Consequently, they should not affect the correlation considerably but rather modify the constants of Eq (4) and (5). The X_{O_2}, however, were changed from 21 to 10 %—a change that can not be easily ignored.

To examine the influence of O_2 concentration, the adiabatic flame temperatures were re-calculated using the "bulk" (average) in-cylinder temperature as the reactant temperature at SOC, in contrast to our earlier use of the maximum "core" temperature. Dec [17] suggests that the periphery of a burning diesel jet is a location where significant NO_x formation occurs. It is conceivable that, in the periphery of the diesel jet, the local gas temperature is between the hot core area and relatively cold outer area. Accordingly, the maximum bulk in-cylinder temperature—estimated by the ideal gas equation—might be a more appropriate initial temperature from which to calculate the peak adiabatic flame temperature. The results obtained with this second approach are shown in Fig. 9, which indicates that

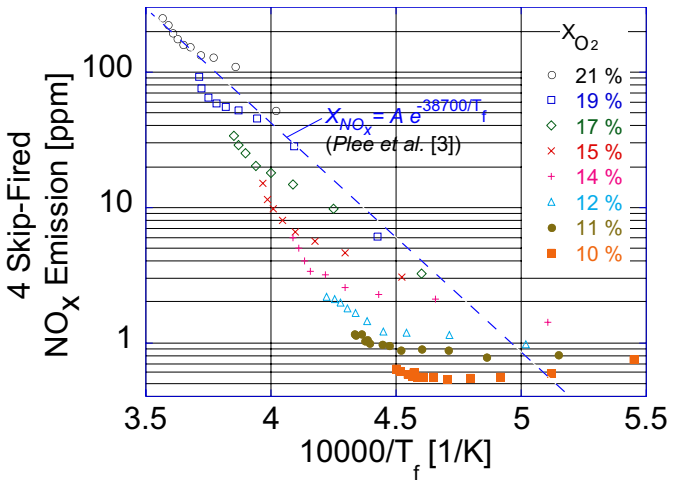

Fig. 9 Correlation of NO_x emission with stoichiometric flame temperature, calculated with the reactants at an initial "bulk" in-cylinder temperature

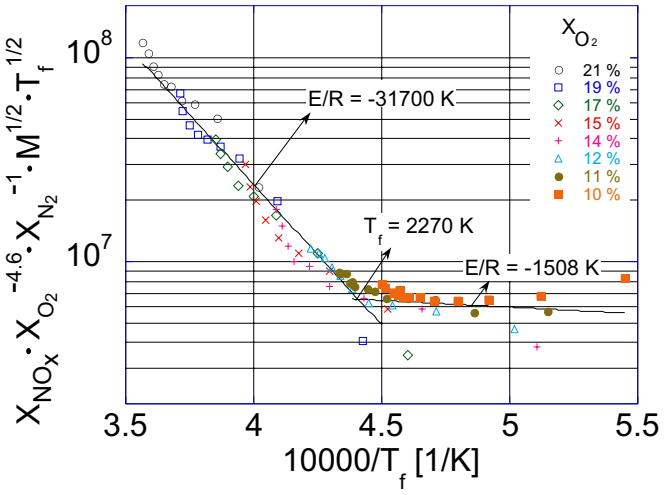

Fig. 10 Correlation of NO_x emission with stoichiometric flame temperature calculated with the reactants at an initial "bulk" in-cylinder temperature, after compensation for the additional parameters suggested by the form of Eq.(2)

Eq. (3) no longer successfully correlates the NO_x emissions and flame temperature. There is an apparent residual dependency on the O_2 concentration.

From Fig. 10, we see a dependency on O_2 concentration to the 4.6 power collapses the data to a single curve rather than 0.5 from Eq. (4). Most of the data where $T_f > 2270\ K$, are well correlated by

$$X_{NO_x} = 7.66\times10^{12} \cdot X_{O_2}^{4.6} X_{N_2} M^{-1/2} T_f^{-1/2} \cdot e^{E_a/RT_f} \qquad (7)$$

where $E_a/R = -31700\ K$. Note the reasonable agreement with the value of E_a/R obtained by Plee and co-workers ($E_a/R = -38700\ K$).

Two regions of differing slope remain, as was observed previously in Fig. 8. In the low-temperature region ($T_f < 2270\ K$), the apparent activation energy is reduced considerably in magnitude and the correlation is better expressed as:

$$X_{NO_x} = 1.27\times10^{7} \cdot X_{O_2}^{4.6} X_{N_2} M^{-1/2} T_f^{-1/2} \cdot e^{E_a/RT_f} \qquad (8)$$

with. $E_a/R = -1508\ K$.

It is clear from the above discussion that it is difficult to accurately predict NO_x emissions from a simple correlation of the form of Eqs.(3) or (6) over the wide range of O_2 concentrations and injection timing considered here. Choice of a single, suitable temperature to employ introduces further complications. Accordingly, simple correlations of the form employed here are best employed to gain an understanding of the important variables influencing NO_x emissions. For a more accurate estimation of actual emission levels, multi-zone models (e.g. [18],[19]), are a more appropriate choice.

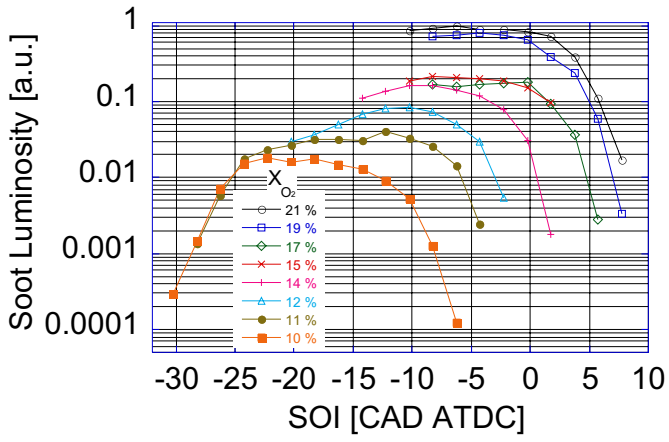

Fig. 11 Effect of O_2 concentration and injection timing on soot luminosity

SOOT LUMINOSITY

As noted in the introduction, engine-out soot emissions typically increase with increasing dilution level. However, beyond a critical dilution level, corresponding to an air-fuel ratio of about 25 [6, 12] or an EGR rate of approximately 55% [13], soot levels are again found to decrease. Because soot oxidation rates are generally thought to decrease with dilution, the decrease in soot at high EGR rates is likely due to reduced formation.

Multi-dimensional modeling studies of soot formation in engines [8] show that for equivalence ratios less than approximately 2, no soot will be formed regardless of the local temperature (see Fig. 1). These numerical results are supported by both experimental engine studies using an oxygenated fuel [20], as well as studies of diesel jets in a constant volume combustion chamber [9]. Moreover, for local temperatures lower than the value required for soot inception (1500–1600K from Fig. 1), no soot is formed whatever the equivalence ratio is. Maintaining low flame temperatures thus has the potential for simultaneously low soot and NO_x emissions.

Figure 11 shows the peak level of spatially-integrated soot luminosity observed during the cycle, measured using the high-sensitivity photodiode shown in Fig. 2. The results were normalized with the maximum value, which occurred at 21% O_2 concentration. The integrated soot luminosity is a complicated function of temperature, the spatial distribution of the soot within the cylinder, and the overall soot volume fraction [14]. A quantitative interpretation of the measured soot luminosity in terms of in-cylinder soot mass is thus not possible. However, fairly simple observations from Fig. 10 can reveal information regarding the soot formation process as dilution or SOI is varied.

A first observation to make from Fig. 11 is that soot luminosity is seen at all O_2 concentrations. Consequently, for our engine compression ratio and inlet conditions, dilution alone does not sufficiently lower flame temperatures to impede the formation of soot. However, we also observe that retarding injection sufficiently at high to moderate EGR rates results in a significant reduction in soot luminosity, suggesting that soot formation can be further suppressed by the additional premixing and the lower flame temperatures associated with the cooling effect of cylinder volume expansion. On the other hand, at 10% O_2 concentration, low soot luminosity can also be achieved at the earliest injection timings. With early injection, however, Fig. 6 demonstrates that the flame temperature is substantially equal (or higher) than those seen at later injection timings. Accordingly, in this case premixing alone is the likely mechanism responsible for reduced soot formation.

IMAGES OF NATURAL COMBUSTION LUMINOSITY

The spatial distribution of soot luminosity, and its temporal evolution, was investigated using the high speed digital video camera. Figures 12, 13 and 14 show pairs of bottom- and side-view images of natural combustion luminosity for 21, 15, and 12% O_2 concentrations, respectively. The apparent heat release rate and the normalized cumulative heat release are shown above the images, with dots indicating the time of image acquisition. The acquisition time, as well as the time of each image after start of injection (ASOI), is superimposed on each image pair. Similarly, the transmissivity associated with the neutral density filter used during the acquisition of each image set is shown on the upper-left image pair.

Several observations are common to the images obtained at all three O_2 concentrations. First, the initial soot luminosity is detected in the latter half of the premixed burn period. This behavior is consistent with the path of conventional diesel combustion discussed in the context of Fig. 1, in which the premixed combustion phase is required to raise the temperature of the mixture to above the soot inception temperature. Second, although some discrete jet structure can be observed in the 21% O_2 soot luminosity distributions, the soot quickly spreads and is more or less uniformly distributed azimuthally by roughly 12 CAD ASOI. Finally, between approximately 12 and 20 CAD ATDC, the bulk of the luminous soot appears to be located within the bowl, but away from the outer periphery. This suggests that the phasing and magnitude of the premixed burning does not significantly affect the flow structures transporting unburned fuel and soot during the mixing-controlled phase of combustion.

In addition to these common features, differences were also observed. As was seen in the integrated luminosity data of Fig. 10, the level of soot luminosity dramatically decreased as the O_2 concentration was decreased (note the increasing filter transmissivity). Additionally, for 21%

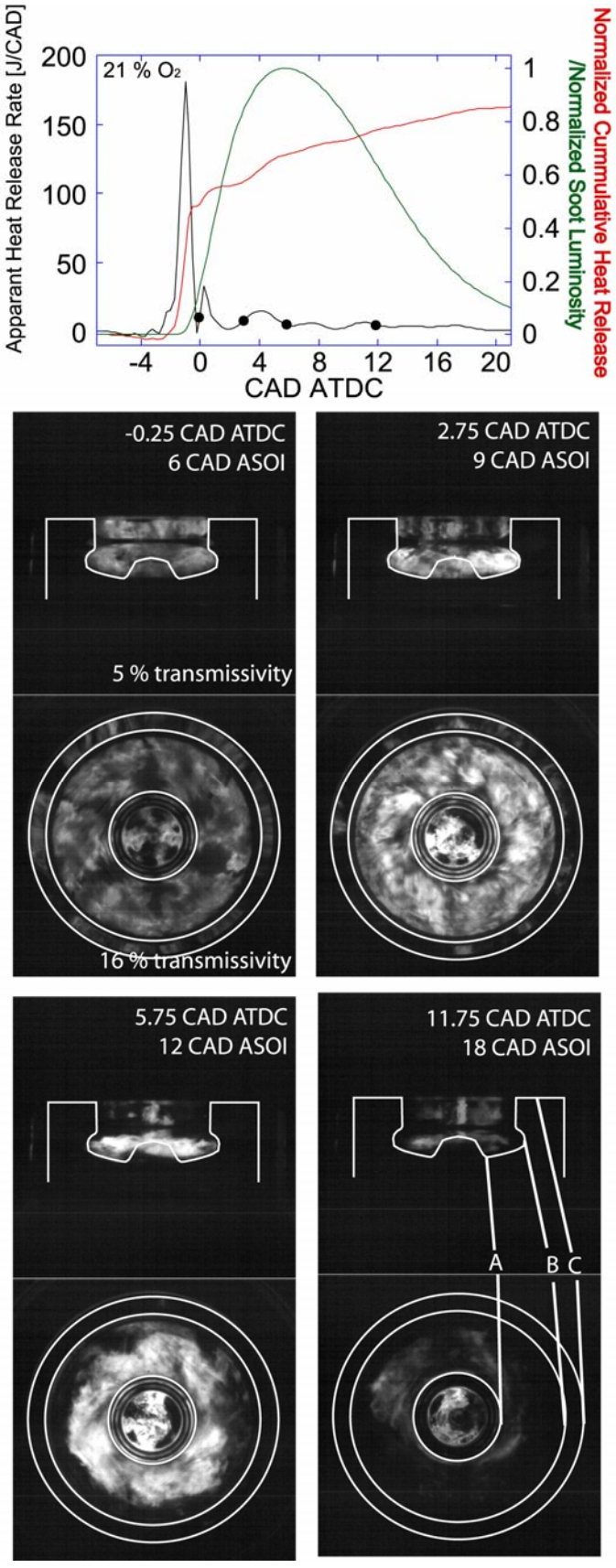

Fig. 12 Images of natural combustion luminosity: -6.25 CAD ATDC SOI, 21% O_2, 30μs exposure time

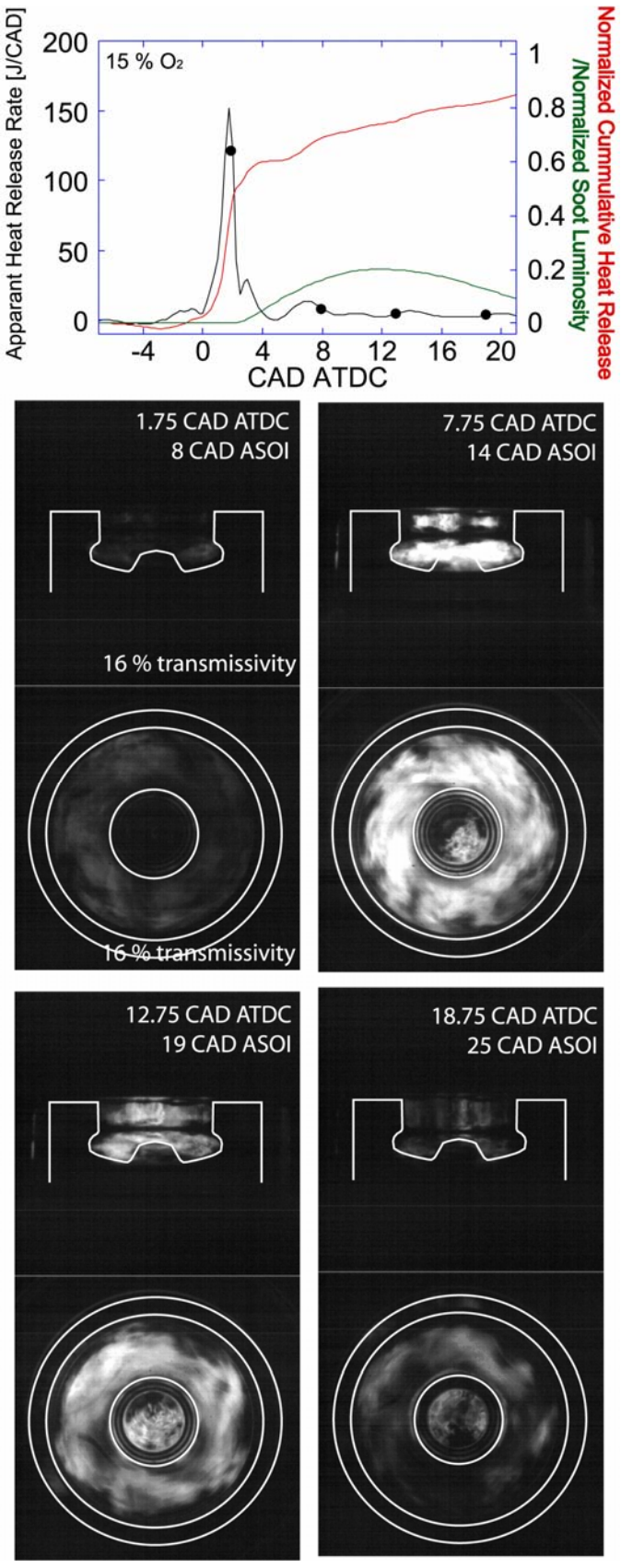

Fig. 13 Images of natural combustion luminosity: -6.25 CAD ATDC SOI, 15% O_2, 30µs exposure time

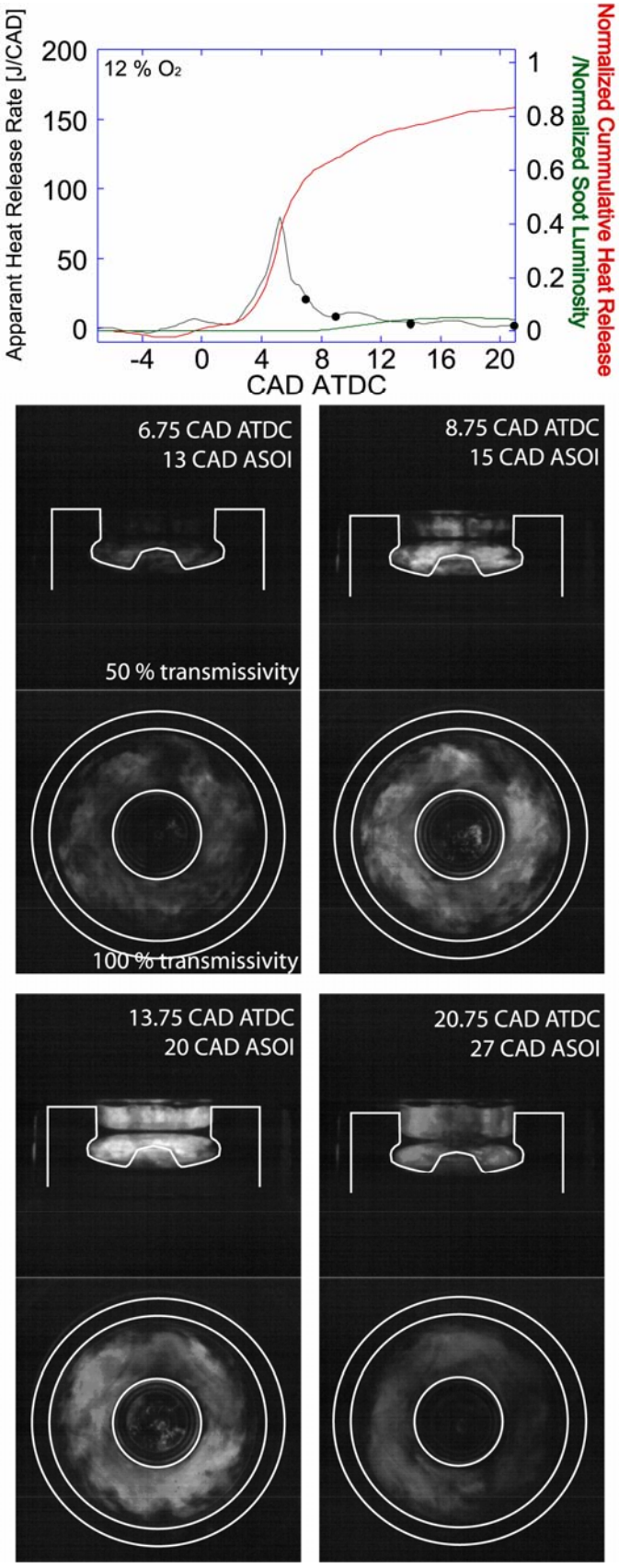

Fig. 14 Images of natural combustion luminosity: -6.25 CAD ATDC SOI, 12% O_2 30µs exposure time

O_2, soot luminosity was detected in the squish area ('B'-'C') at early crank angles (-0.25 and 2.75 CAD ATDC). However, soot luminosity in the squish area appeared later (12.75 CAD) at 15 % O_2 concentration and did not appear at 10% O_2 concentration. These differences in the squish area soot luminosity suggest differences in the soot formation rates in this region for the different O_2 concentrations.

CO EMISSIONS

CO emissions are typically small for conventional, high-temperature diesel combustion strategies. With high combustion temperatures, CO is easily oxidized even though large amounts of CO are formed during the premixed burning of fuel-rich regions [21]. On the other hand, low-temperature combustion systems often exhibit high CO emissions, particularly at high dilution levels. There remains some question as to the source of these CO emissions. Due to the extended ignition delay encountered in low-temperature systems, significant portions of the fuel could mix to very lean equivalence ratios ($T_f < 1500\,K$). Under these "over-mixed" conditions, combustion temperatures are too low for the oxidation of CO to be completed on engine time scales [22]. "Over-mixed" fuel has been shown to be the dominant source of CO emissions for conventional diesel combustion [21].

On the other hand, the presence of soot (discussed above) implies that some fraction of the premixed combustion occurs under fuel-rich conditions. Combustion of this "under-mixed" fuel will produce copious amounts of CO (and H_2). Completion of combustion (burn-out of the CO formed) is conditional on additional mixing of the products of rich combustion with oxidant. This mixing process is more difficult to complete quickly with low O_2 concentrations, due to the need to mix with a greater volume of ambient fluid. Additionally, the lower flame temperatures of diluted mixtures imply that less time is available before expansion drops the temperature below a threshold level required for sufficiently rapid CO oxidation.

Measured CO emissions are shown in Fig. 15. At low-to-moderate dilution levels ($X_{O_2} \geq 17\,\%$), the CO emissions correlate strongly with the ignition delay results presented below (see Fig. 16), increasing with both increased diluent and retarded SOI. This observation, coupled with the numerical results of [21] and the general inverse correlation of the CO emissions with the peak flame temperature (Fig. 6), suggests that the incomplete combustion of "over-mixed" fuel is the dominant mechanism responsible for the CO emissions at low EGR rates. However, the inverse flame temperature correlation is also consistent with CO emissions from the products of combustion of "under-mixed" fuel. Furthermore, as O_2 concentrations decrease, the CO emissions begin to correlate inversely with ignition delay. At high dilution rates it thus appears more probable that CO emissions originating from "under-mixed" fuel dominate. A correlation of CO emissions with the average in-cylinder temperature late in the combustion process, discussed below, further reinforces this view.

At low-to-moderate dilution levels and retarded injection timing, charge cooling and low flame temperatures may impede the burn-out of the CO formed in the rich pre-mixed combustion, and additional numerical simulations and/or in-cylinder measurements will be required to clarify the dominant source of the CO emissions

IGNITION DELAY

Ignition delay is influenced by both physical and chemical factors, and is thus affected by characteristics of the fuel injection equipment (injection pressure, nozzle hole diameter), injection timing (ambient temperature and density) and charge dilution (EGR rate) [22, 23]. Here,

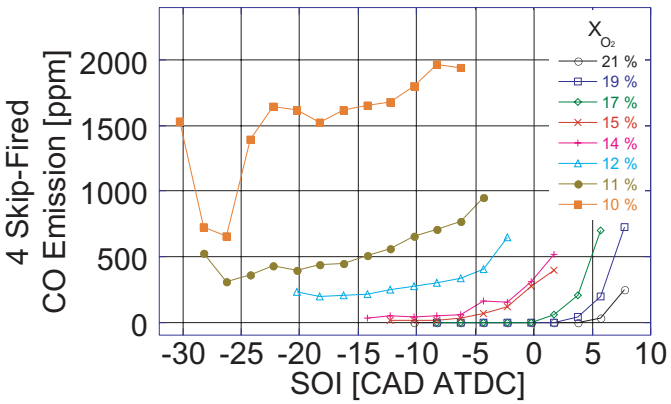

Fig. 15 Effect of O_2 concentration and injection timing on CO emission

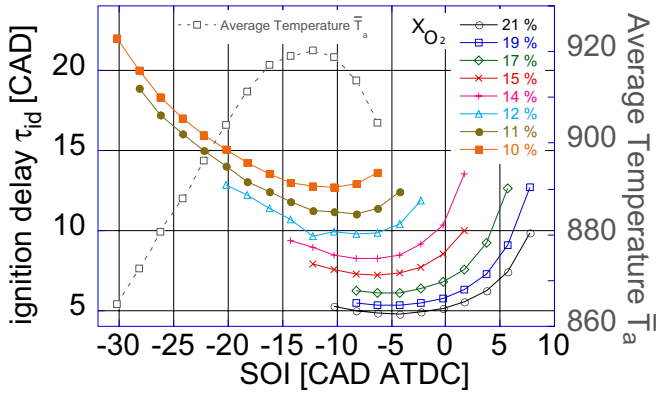

Fig. 16 Effect of O_2 concentration and injection timing on ignition delay together with the average ambient temperature estimated for an O_2 concentration of 10%

ignition delay is defined as the time from SOI to start-of-combustion (SOC), as determined by the crank angle at which 10% of the cumulative heat release occurred. This crank-angle correlates well with the beginning of rapid, high-temperature heat release.

Figure 16 shows that, at the same injection timing, the ignition delay increases with decreasing O_2 concentration. To isolate the effect of O_2 concentration from the effects of changing ambient temperature or density as the dilution level is increased, the temperature and density of the ambient gas were maintained at the same value regardless of O_2 concentrations (see Fig. 4 and the accompanying discussion).

As the injection timing is varied, the ignition delay varies inversely with the estimated average in-cylinder temperature $\overline{T}_a$

$$\overline{T}_a = \frac{T_{SOI} + T_{SOC}}{2} \tag{9}$$

where T_{SOI} is the bulk in-cylinder temperature at SOI and T_{SOC} is bulk in-cylinder temperature at SOC. T_{SOI} was estimated from the ideal gas law using the known pressure and volume history, an estimated reference temperature at TDC (without combustion), and the assumption of a fixed mass. The reference temperature at TDC was taken to be the typical bulk gas temperature, and was estimated based on the value calculated from multi-dimensional numerical calculation [10]. With this procedure for estimating temperature, the peak temperature occurs earlier than the peak pressure, due to heat loss during compression. For example, the peak in-cylinder temperature at 10% O_2 concentration was around -12 CAD ATDC, which was near the crank angle where the shortest ignition delay was measured. The bulk in-cylinder temperature T_{SOC} was estimated from the cylinder pressure at the reference state assuming an isentropic compression or expansion process. This observed effect of ambient temperature on ignition delay is well-known—an increase in temperature shortens the ignition delay [23].

To examine the influence of $\overline{T}_a$ more closely, the ignition delay τ_{id} is plotted on a logarithmic axis against $\overline{T}_a^{-1}$ in Fig. 17. Here it is seen that τ_{id} increases exponentially with $\overline{T}_a^{-1}$. Two additional observations are noteworthy. First, an apparent dependency of ignition delay on O_2 concentration clearly remains. Second, at fixed O_2 concentration, the same τ_{id} is measured for two different $\overline{T}_a$. The latter observation shows that the ignition delay cannot be expressed with $\overline{T}_a$ alone, even at constant X_{O_2}. However, ignition delay is also known to be

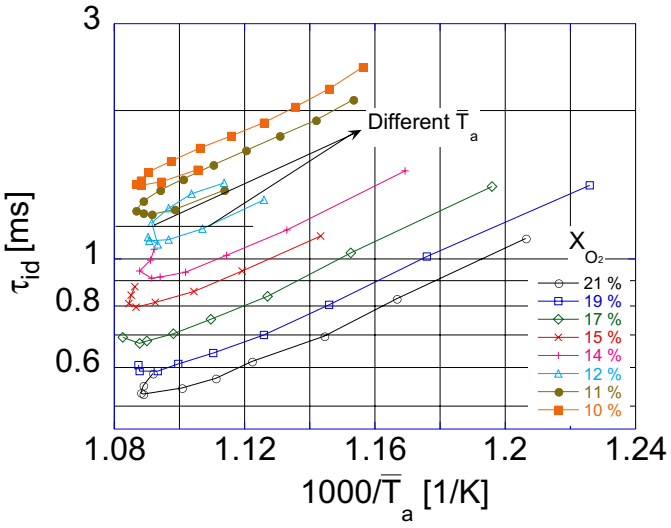

Fig 17. Correlation of ignition delay with average ambient temperature

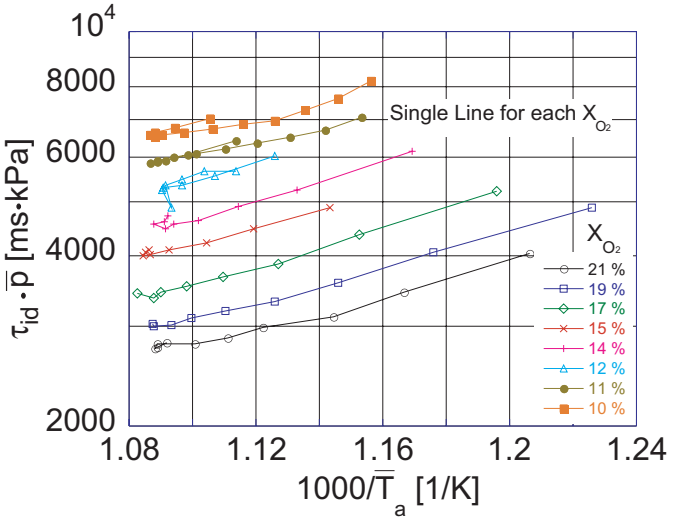

Fig. 18 Correlation of ignition delay with average ambient pressure and temperature

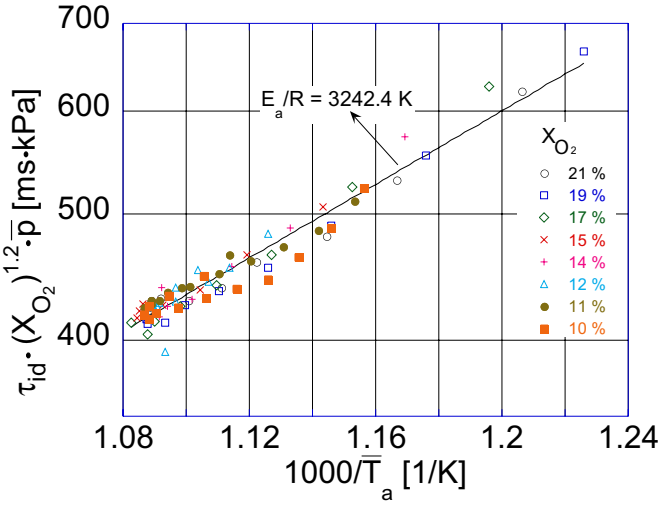

Fig. 19 Correlation of ignition delay with average ambient pressure, temperature and O_2 concentration

influenced by ambient pressure, and correlations for ignition delay measured in constant pressure and temperature environments are typically of the form [24]:

$$\tau_{id} = A \cdot \overline{p}^{-n} \cdot e^{E_a / R\overline{T}_a} \quad ms \qquad (10)$$

A and n are constants dependent on fuel and airflow characteristics, p is the ambient pressure, R is the universal gas constant, and E_a/R is an apparent activation energy for the auto-ignition process. The constant n is typically close to 1.

The influence of pressure (with n = 1) on ignition delay is illustrated in Fig. 18, where $\tau_{id} \cdot p^n$ is plotted against $\overline{T}_a^{-1}$. Now, for fixed O_2 concentration, a single ignition delay is predicted at each temperature. However, a significant dependency on X_{O_2} remains. Consequently, we have included the influence of O_2 concentration on ignition delay by considering the following expression:

$$\tau_{id} = 12.254 \cdot \overline{p}^{-1} \cdot X_{O_2}^{-1.2} \cdot e^{E_a / R\overline{T}_a} \quad ms\,,\ E_a / R = 3242.4\ K \qquad (11)$$

As can be seen in Fig. 19, Eq.(11) effectively predicts the ignition delay at all O_2 concentrations. From this equation, we see that ignition delay is decreased not only by fuel injection into high ambient pressures and temperatures, but also by high O_2 concentrations. The latter dependency is to be expected due to the slowing of chemical reactions in dilute mixtures, as well as the decreased temperature rise from early low-temperature reactions due to the heat capacity of the diluent molecules.

EQUIVALENCE RATIO AT IGNITION

As can be inferred from Fig. 1, the equivalence ratio at ignition will influence the typical path followed by a fuel element in the ϕ-T plane as the combustion process progresses, thereby affecting soot and NO_x formation. By changing the dilution level, we anticipate that the equivalence ratio at ignition will change due to the following two opposing factors:

1. Ignition delay: As shown in the previous section, decreased O_2 concentrations resulted in increased ignition delay, allowing a greater time period for premixing to occur. For example, at the same injection timing, the ignition delay observed with 10% O_2 concentration can be over twice as great as is seen for O_2 concentrations of 17% and above.

2. Low ambient O_2 concentration: Due to the decreased O_2 concentration, a greater amount of ambient fluid must be mixed with the fuel to achieve the same fuel-air equivalence ratio. For example, at 10% O_2 concentration, over twice the volume of ambient fluid must be mixed with the fuel to achieve the same fuel/O_2 ratio as for 21% O_2.

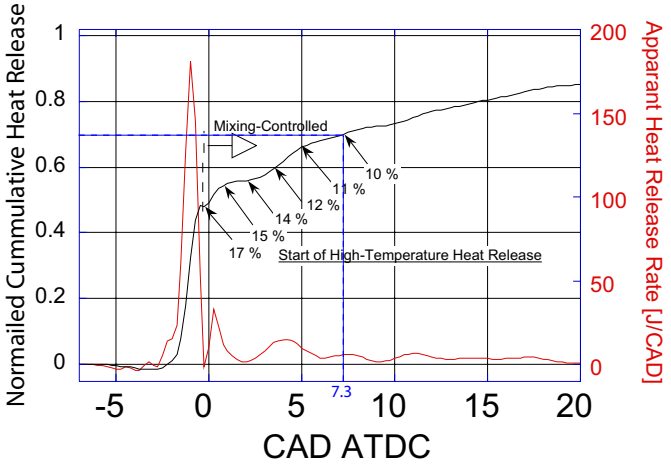

Fig. 20 Estimation of the percentage of premixed O_2

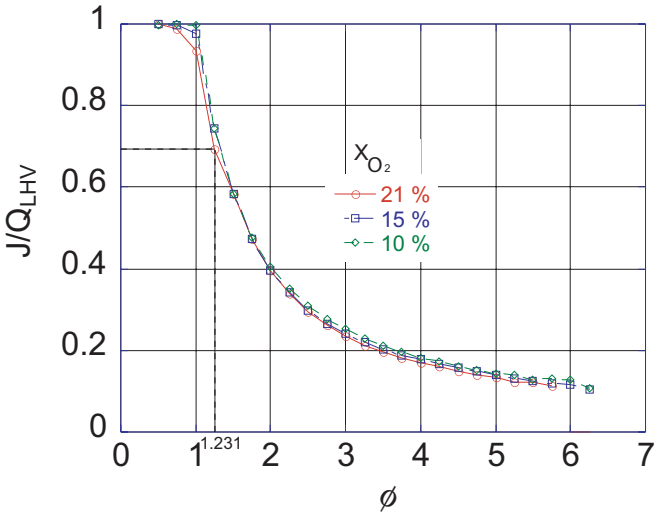

Fig. 21 The fraction of the energy released as a function of the equivalence ratio (SENKIN calculation after high-temperature ignition, ambient temperature = 900K, Fuel temperature = 373K)

Studies of flame lift-off in free jets [25] show that as O_2 concentrations are reduced, the flame lift-off increases such that the average mixture equivalence ratio at lift-off remains approximately constant. Assuming that flame lift-off is dominated by ignition-like processes, we might suppose that the opposing effects of increased ignition delay and reduced O_2 concentration identified above would be largely self-canceling. However, steady-state mixing rates in a free jet and the average mixing rates in our short injection-duration, transient engine experiments are likely to be significantly different, and such a supposition cannot be justified.

An estimate of the equivalence ratio at ignition can be made, however, through examination of the cumulative heat release observed with 21% O_2. With 21% O_2, the rates of chemical reaction are fast and—beyond the

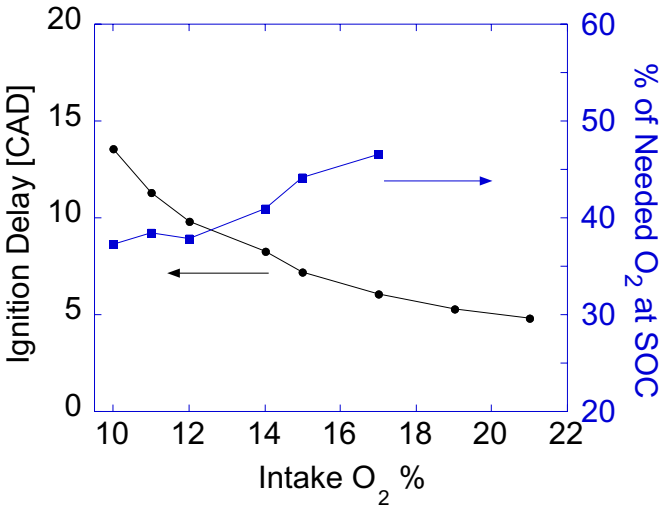

Fig. 22 Ignition delay and the fraction of premixed O_2 present at SOC

premixed burning period—the cumulative heat release can be correlated with the fraction of O_2 needed for complete combustion which has been mixed with the fuel. We also assume that, given the same SOI and bulk temperature, the fuel/ambient gas volumetric mixing rates are substantially independent of O_2 concentration or the presence of heat release. With these approximations, a measure of the 'average' equivalence ratio at ignition for the various dilute mixtures can be obtained by examination of the 21% O_2 cumulative heat release (measured at the same SOI) at the crank angle that the dilute mixture ignites.

The estimated equivalence ratio at ignition for the lower O_2 concentrations is obtained from Figures 20 and 21 using the following procedure: First, the crank angle at which high temperature heat release begins is determined for the dilute combustion case being considered. At this crank angle, the normalized cumulative heart release for the 21% O_2 case is determined from Fig. 20, and the corresponding equivalence ratio (or fraction of needed O_2) is then found from Fig. 21. It is notable that the fractions of energy released at a given equivalence ratio are identical for different O_2 concentrations. Finally, the fraction of needed O_2 is multiplied by the ratio of stoichiometric air-fuel ratios to account for the lower O_2 concentration of the dilute case. This procedure could not be followed for the case of 19% O_2, as ignition occurred before the onset of mixing-limited combustion for 21% O_2.

For example, at 10% O_2 concentration, ignition occurred at 7.3 CAD ATDC. At this crank angle, Fig. 20 indicates that 70% of the cumulative heat release is observed in the 21% O_2 case, corresponding to (from Fig. 21) an equivalence ratio of 1.231 or about 81 % of the needed O_2. In the dilute case, however, the fraction of needed O_2 will be considerably lower, and it is necessary to multiply by the ratio of stoichiometric fuel-air ratios given in Table 3—(14.5/31.6). Consequently, only about 37% of the needed O2 is present at ignition for 10% O_2.

Figure 22 shows the results of this estimation and the ignition delay for data obtained at -6.25 CAD ATDC SOI. Note that the fraction of O_2 needed for complete combustion does not increase as the O_2 concentration decreases, despite the increasing ignition delay. On the contrary, we observe an increase in the equivalence ratio at ignition for more dilute mixtures. Consequently, if a leaner equivalence ratio at ignition is desired, modifying the ambient gas temperature (through modified injection timing, compression ratio, or intake charge cooling) to increase ignition delay appears a better strategy than employing dilute mixtures. As will be seen below, a simple adiabatic mixing argument supports the above observations of increased ϕ at ignition for dilute mixtures, as well as the effectiveness of ambient temperature in modifying ϕ at ignition.

APPARENT COMBUSTION DURATION

Figure 23 shows the time from the start of rapid heat release until one-half of the total apparent heat release has occurred—the 10-50% burn time. This parameter is of interest for two reasons. First, it provides information on the path of the combustion process in the ϕ-T plane. For rapid premixed burning, very little additional mixing takes place during the premixed burning portion of the combustion path shown in Fig. 1. However, the early combustion duration can increase 5-fold for high dilution levels and/or retarded injection timing. Under these circumstances, it is anticipated that significant additional mixing can occur between SOC and the time the peak combustion temperatures are achieved at the end of premixed burning. Second, the 10–50% burn period is typically found to vary inversely with the peak heat

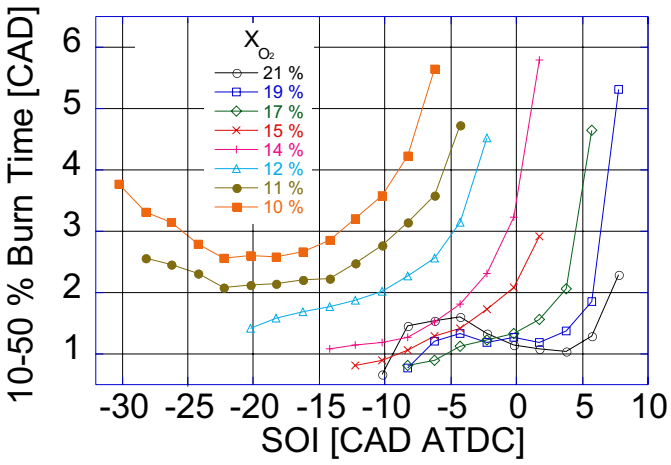

Fig. 23 Effect of O_2 concentration and injection timing on 10-50 % burn time

release rate, and thus also correlates inversely with combustion noise. Accordingly, Fig. 23 demonstrates that at the highest EGR rates ($X_{O_2} \leq 12\%$), significant reductions in combustion noise can be expected regardless of injection timing, while at more moderate dilution levels retarded injection timing will be required to moderate the premixed heat release rate.

The behavior of the 10-50% burn times as SOI is varied is reminiscent of the ignition delay behavior seen above (Fig. 16), particularly at the highest dilution levels. It seems reasonable to expect, then, that some correlation between the burn time and the average in-cylinder temperature during the 10–50% burn period would be observed. In general, such a correlation does exist, but is imperfect. In particular, the increase in burn time at advanced SOI at high dilution levels, and the complex

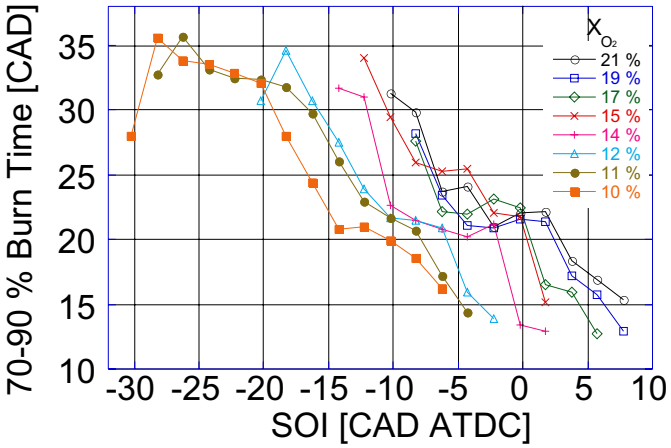

Fig. 24 Effect of O_2 concentration and injection timing on 70-90 % burn time

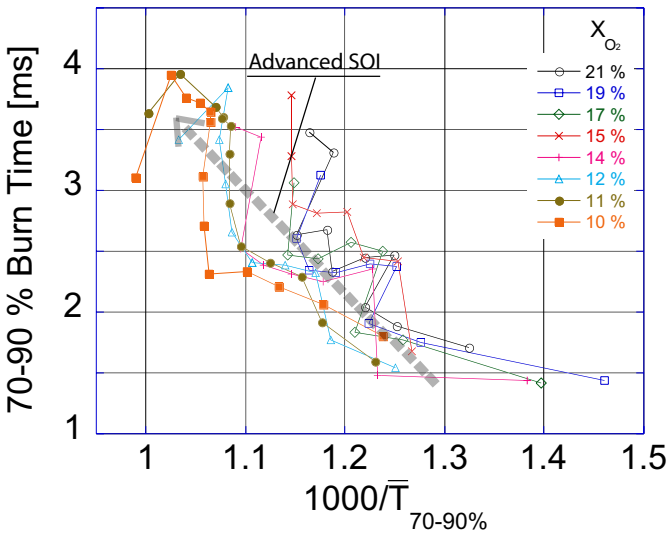

Fig. 25 Correlation of the 70-90% burn time with the bulk in-cylinder temperature during this period

behavior at low dilution levels cannot be correlated well with the average temperature. We believe that mixture preparation issues, including wall-wetting effects, may be influencing these results as well.

The 70-90% burn times, a measure of the time period spent in the latter, mixing-controlled portion of the combustion path of Fig. 1, are presented in Fig. 24. It seems clear that the decreased burn time (at fixed SOI) observed for more dilute mixtures is inconsistent with a mixing-controlled heat release process. Similarly, the decreased burn time observed with retarded injection, when average combustion temperatures are lower due to cylinder volume expansion, seems inconsistent with a kinetically-controlled process.

To examine this more closely, we have correlated the 70-90% burn times with the average in-cylinder temperature during this period. The results are shown in Fig. 25, where it is apparent that, overall, slower apparent burning occurs at the higher average temperatures. This behavior is consistent with the expectation that heat transfer losses will be higher for higher bulk gas temperatures, leading to lower apparent heat release rates, as expressed in Eq.(1). As discussed previously [10], we thus conclude that, as dilution or injection timing are varied, changes in the heat transfer losses influence the apparent heat release more than changes in the actual chemical heat release rate (Eq.(1)).

In closing, it is noteworthy that the general trend of increased CO emissions with retarded injection timing correlates well with the bulk in-cylinder temperature during the 70–90% burn period, as would be expected if these emissions are dominated by “under-mixed” fuel, and CO oxidation rates are lowered by falling temperatures before sufficient mixing of partially-burned fuel can occur.

FUEL CONVERSION EFFICIENCY

As demonstrated by the emissions measurements discussed above, low NO_x and low peak soot luminosity are achievable with low-temperature combustion in a diesel engine. However, large increases in CO emissions at high dilution levels or retarded injection timing raise the issue of whether this low-temperature combustion can be achieved with a reasonable penalty in fuel economy. In this section, we examine the various factors influencing the fuel conversion efficiency to help clarify this issue.

The indicated fuel conversion efficiency η_{fc} is the ratio of the indicated work W to the chemical energy in the injected fuel, calculated from the product of the fuel mass and the lower-heating value Q_{LHV} of the fuel [24]

$$\eta_{fc} = \frac{W}{m_f Q_{LHV}} \tag{12}$$

Figure 26 shows the measured η_{fc} for all of the operating conditions discussed above. Notice that a distinct maximum η_{fc} is observed near 14% O_2 concentration and SOI around -5 CAD ATDC. To identify the source of this result, it is useful to decompose the fuel conversion efficiency into separate contributions which stem from distinct physical processes. Accordingly, we extend the analysis of Kimura and co-workers [11], and write η_{fc} as a product of three separate efficiencies

$$\eta_{fc} = \frac{W}{m_f Q_{LHV}} = \left(\frac{W}{Q_{chem} - Q_{hl}}\right)\left(\frac{Q_{chem} - Q_{hl}}{Q_{chem}}\right)\left(\frac{Q_{chem}}{m_f Q_{LHV}}\right) \tag{13}$$

The term $Q_{chem} - Q_{hl}$ is the difference between the total chemical heat release and the heat transfer losses, and is equal to the integral of the apparent heat release rate Q_{total} (see Eq. (1)). Consequently, the first term on the right-hand-side of Eq.(13), η_{wc} , represents the efficiency with which the total apparent heat release is converted to indicated work. This term is related to the combustion phasing.

The second term

$$\eta_{hl} = \frac{Q_{chem} - Q_{hl}}{Q_{chem}} = 1 - \frac{Q_{hl}}{Q_{chem}}, \tag{14}$$

is related to the fraction of the total chemical heat release lost by heat transfer, or, equivalently, a “heat-loss” efficiency. Finally, assuming no further heat release takes place after exhaust valve opening, the last term is equal to the combustion efficiency η_c . The work conversion efficiency can be computed directly from the measured pressure data, and the combustion efficiency is estimated from

$$\eta_c = 1 - f\left(\frac{\Delta h^0_{f,CO} - \Delta h^0_{f,CO_2}}{\Delta H_R}\right) \tag{15}$$

In Eq.(15), f represents the fraction of fuel carbon found in the CO emissions, ΔH_R is the negative of the fuel lower heating value, and Δh^0_f is the heat of formation of the sub-scripted species. Combustion efficiencies estimated from Eq.(14) will be high, due to the neglect of the energy tied up in unmeasured species, principally H_2 and unburned hydrocarbons.

The estimated combustion efficiency and the work conversion efficiency are shown in Figs. 27 and 28, respectively. From Eq.(12), we can also reconstruct a map of the heat-loss efficiency required to produce the measured fuel conversion efficiencies. However, in using this map to interpret the trends in the fuel conversion efficiency data, it is important to recognize that, due to the neglect of the H_2 and unburned hydrocarbons in the estimation of the combustion efficiency, the results are

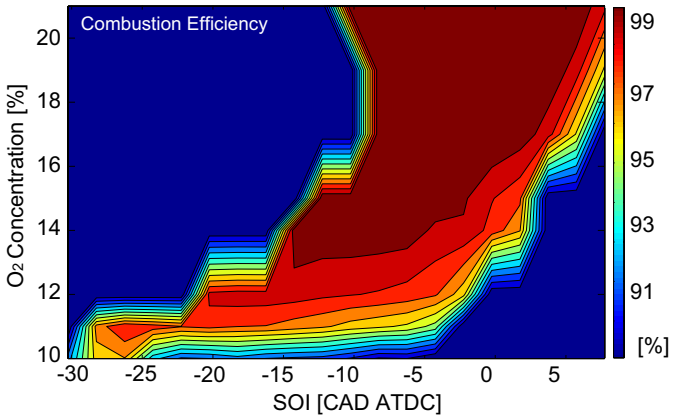

Fig. 27 Effect of O2 Concentration and injection timing on combustion efficiency

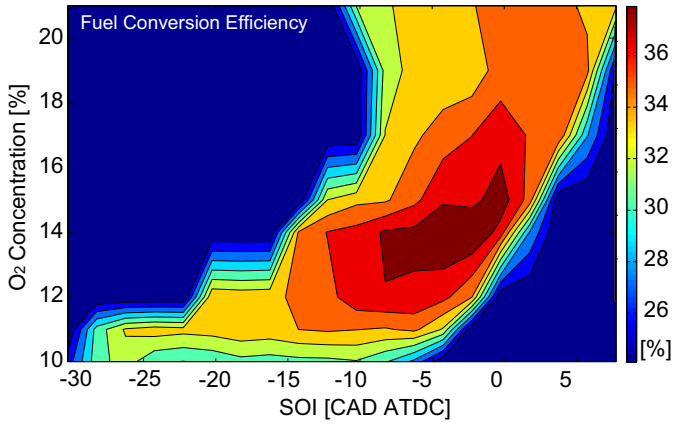

Fig. 26 Effect of O_2 concentration and injection timing on fuel conversion efficiency (Eq. 12)

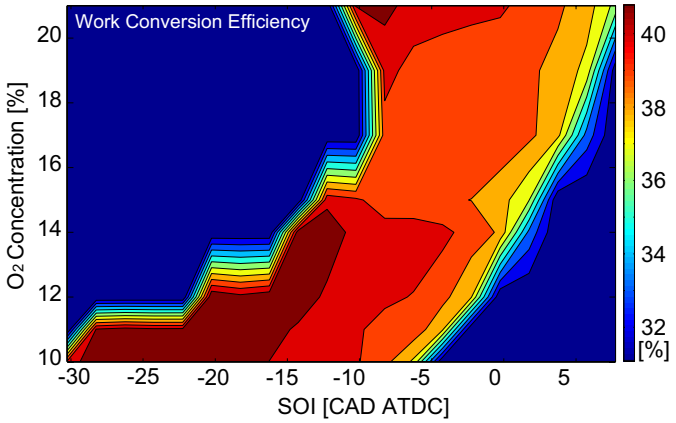

Fig. 28 Effect of O2 Concentration and injection timing on work conversion efficiency

most reliable only in regions where our combustion efficiency estimate is near unity. Although the data is partly limited, from these figures, it is possible to identify the dominant factors influencing the fuel conversion efficiency.

At low O_2 concentration or retarded injection timing, combustion efficiencies are low. In contrast, high work conversion efficiencies are observed at low O_2 concentration, due to the ability to inject earlier. Although heat release occurring prior to TDC lowers η_{wc}, the benefit of shifting the overall combustion phasing earlier overwhelms this disadvantage. These higher work conversion efficiencies (comparable to η_{wc} achieved at 21% O_2 concentration and optimal injection timing) cannot compensate for the low η_c, however, and at low O_2 concentration η_{fc} drops. At retarded SOI, both decreased η_c and decreased η_{wc} lead to lower η_{fc}.

At moderate dilution levels and injection timing that is not excessively retarded, both η_c and η_{wc} remain relatively constant, and cannot explain the decrease in η_{fc} from its peak value, which occurs as SOI is advanced or dilution decreases. However, at fixed dilution, advancing SOI can be observed to increase the calculated peak adiabatic flame temperature T_f (Fig. 6), which will likely increase both convective and radiation heat transfer losses. With earlier injection, more time is available for heat transfer to occur, and hot combustion gases are present near TDC when combustion chamber surface-area-to-volume ratios are high. Further, Fig. 25 indicates that bulk gas temperatures in the 70–90% burn period increase as SOI is advanced, suggesting higher heat losses in the latter stages of combustion.

In like manner, we can also expect increased heat transfer losses due to the large increases in T_f that occur as dilution levels drop (at fixed SOI), as well as enhanced losses due to the advanced combustion phasing associated with the decreased ignition delay. Overall, it seems plausible that increased heat transfer losses are responsible for the decreased η_{fc} as either SOI is advanced or dilution is increased. The impact of these various factors on η_{fc} is summarized in Table 5.

Table 5 The influence of charge dilution on the fuel conversion efficiency and its component efficiencies

X_{O_2}	η_c	η_{wc}	η_{hl}	η_{fc}
High	↑	-	↓	-
Moderate	↑	-	↑	↑
Low	↓	↑	↓	↓

↑: High, -: Moderate, ↓: Low

POSTULATED COMBUSTION PROGRESS IN THE ϕ-T PLANE

As a first step to collecting the results presented above and using them to sketch the progress of the combustion process in the ϕ-T plane, it is useful to examine the pre-ignition mixture preparation process in greater detail. A simple adiabatic mixing analysis provides additional insight into this process, as is illustrated in Fig. 29. In the upper left portion of the figure are shown three paths, corresponding to the ϕ-T history of a fuel parcel as it mixes with ambient fluid at three different O_2 concentrations. If the mixing process were to continue without heat release, each of these paths would converge on the assumed ambient temperature—900 K. However, between roughly 800 and 850 K [26], the low-temperature heat release becomes significant, and the path departs from the adiabatic mixing path. Note that the mixing path characteristic of low ambient O_2 concentrations reaches the mixture temperature at which heat release becomes significant at a higher equivalence ratio, due to the heat capacity of the diluent molecules.

For the 21% O_2 concentrations, this initial heat release occurs over very short times, as evidenced by the absence of a separate low-temperature heat release region in the measured apparent heat release rates (or in the in-cylinder pressure records, as noted in the discussion surrounding Fig. 4). Consequently, little additional mixing is expected to occur before a temperature of about 1000 K is reached, when rapid, high-temperature heat release commences. That is, chemical reaction time scales are much less than mixing time scales along this path segment. With increased dilution, the rate of initial temperature rise is lower, due to both the heat capacity of the diluent molecules and the expectation that heat release rates are lower due to the

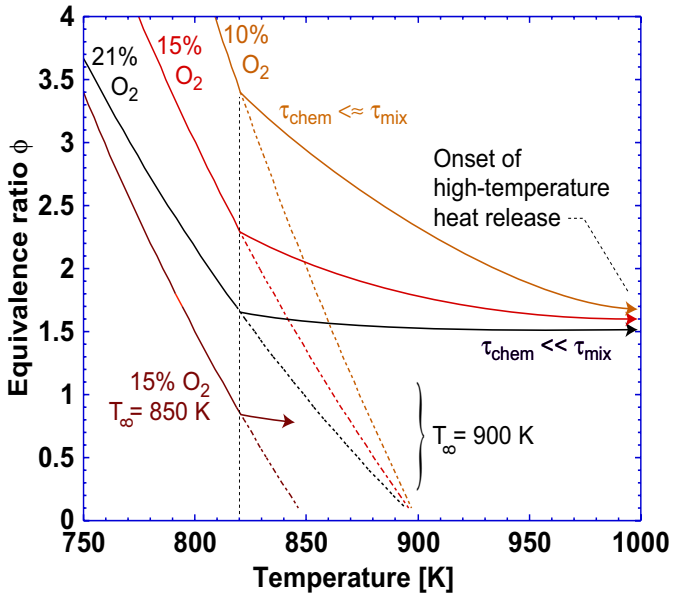

Fig. 29 The path of a fuel parcel in the ϕ-T plane corresponding to an adiabatic mixing process followed by low-temperature heat release

lower reactant concentrations (see the influence of O_2 concentration on ignition delay discussed above). Accordingly, we anticipate that significant additional mixing can occur during the time period between the inception of low-temperature heat release and the onset of high-temperature heat release at 1000 K. The mixture equivalence ratio estimates at ignition (Fig. 22) support this picture— the estimated ϕ at SOC was increased with increased dilution when SOI was held fixed.

Before proceeding to a more complete description of the combustion path, a final observation should be made from the simple mixing analysis of Fig. 29: ambient temperature can be expected to exert a large influence on the equivalence ratio at the start of low-temperature heat release. With an O_2 concentration of 15%, a nearly 3-fold decrease in equivalence ratio at the start of low-temperature combustion is observed when the ambient temperature is reduced to 850 K. This corresponds to roughly a 20 K reduction in intake temperature at our compression ratio of 18.7, or, equivalently, a reduction in compression ratio to about 15.6.

In Fig. 30 we reproduce the ϕ-T plane diagram of Fig. 1, depicting the soot and NO_x formation areas based on the numerical results of Ref. 8. We also show on the plot the maximum temperature achieved when a homogeneous mixture of fuel and air at the specified equivalence ratio and an initial temperature of 1000 K is burned. For very rich mixtures ($\phi > \approx 2$), this temperature can exceed the equilibrium flame temperature by several hundred degrees before endothermic reactions lower the final temperature to its equilibrium value. Finally, the line demarcating regions of fast and slow CO oxidation is reproduced from Ref. 21. In the fast CO oxidation regions, equilibrium CO concentrations are reached in less than 1 ms.

The paths followed by typical fuel parcels, as they mix and burn, are considered in Fig. 30 for two common low-temperature combustion systems. The first is characterized by late-injection and moderate dilution levels (similar to the Nissan "MK" system), and the second is characterized by higher EGR rates and earlier injection (similar to the AVL "HCLI" system). Also shown in Fig. 30 is a typical path for conventional diesel combustion (reproduced from Fig. 1), illustrated by the open gray arrows. For late-injection combustion systems we consider the path marked 'A'. Under these operating conditions, SOI was near TDC, and the O_2 concentration was approximately 15%.

Figures 22 and 29 indicated that, at fixed SOI (or ambient temperature), the equivalence ratio at the start of rapid, high-temperature combustion remained nearly the same as O_2 concentrations were decreased. However, due to the retarded injection timing, in-cylinder temperatures during the ignition delay period are lower than for conventional diesel combustion. The lower ambient temperatures will promote mixing to a leaner equivalence ratio prior to the onset of low-temperature heat release (Fig. 29), as well as an increase in the overall delay before the onset of high-temperature heat release (Fig. 16). Overall, we thus expect a leaner typical mixture equivalence ratio at SOC than is found for conventional diesel combustion.

At SOC, the path segment representing the premixed burn period begins. Figure 23 indicates that, due primarily to the retarded combustion phasing, the premixed burn time is approximately 50% greater than is observed for conventional diesel combustion dilution levels and injection timings. Accordingly, we expect some additional mixing to take place during the premixed burning, a process which is represented by the small negative slope of the premixed path segment. Due to the late combustion phasing, cylinder volume expansion is cooling the charge, and the peak combustion temperatures do not reach the maximum flame temperature line computed for a constant 1000 K ambient temperature at the 15% O_2 concentration. At the end of the premixed path segment the formation of soot is expected to be greatest, due to the proximity of the fuel parcel to the soot formation regions. As noted from the measurement of soot luminosity, the first occurrence of luminous soot is not observed until well into the premixed combustion phase.

As the subsequent mixing-controlled combustion takes place, the path departs still further from the maximum flame temperature curve due to continued cooling by volume expansion. Along this path segment, CO, H_2, and other products of the rich premixed combustion are oxidized as mixing proceeds. We also anticipate that

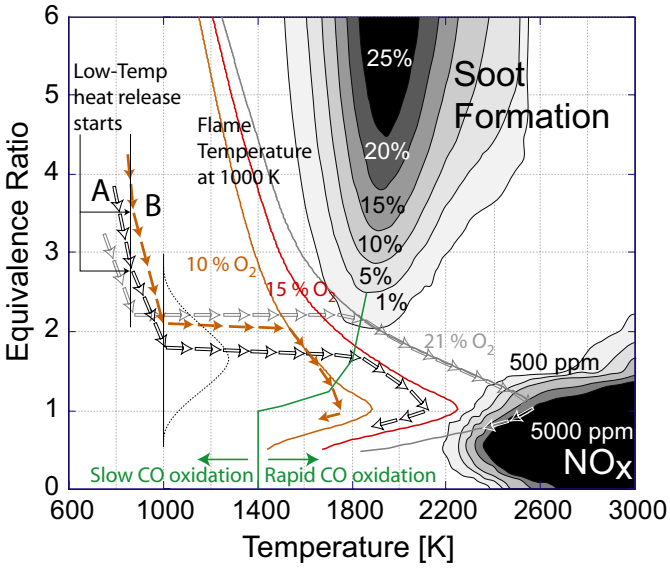

Fig. 30 Postulated path for two low-temperature combustion modes in the ϕ-T plane

some soot oxidation occurs by OH radical attack, even in the absence of significant quantities of oxygen.

The combustion behavior described above is advantageous for low soot and NO_x formation. Peak temperatures associated with the early heat release are kept low by formation of rich mixtures during the ignition delay period, when rapid mixing, driven by the fuel injection process, takes place. Later, the slower mixing rates associated with the in-cylinder fluid dynamics allow expansion and cooling to occur before the peak combustion temperatures are reached, thereby avoiding the NO_x formation regions. However, mixing must be completed before temperatures drop below those at which CO oxidation slows. To accomplish this, mixing rates must be kept high even though the bulk of the energy provided by the fuel injection event has dissipated.

Finally, before proceeding with a discussion of the early-injection system, we note that there will be a broad distribution of equivalence ratios present in the cylinder at ignition, as indicated by the dashed distribution function sketched on the figure. Ignition of the richer mixtures, with relatively low mixture temperatures, will be facilitated by compression heating caused by the pressure increase when the first fuel parcels begin to ignite. In particular, we note that the presence of in-cylinder soot in Figs. 12–15 indicated that the distribution of equivalence ratios must include significant regions with $\phi > 2$. The path sketched in Fig. 30 is thus not unique, but rather representative of a typical fuel parcel.

A path more characteristic of early-injection, high dilution combustion systems is shown by the solid arrow in Fig. 30. Typical operating conditions for this path are 10% O_2 concentration (65% EGR at this load) and SOI at -20 CAD ATDC. The beginning of the initial adiabatic mixing segment of this path is labeled 'B'. Due to the lower O_2 concentrations, but similar average ambient temperatures during the ignition process (Fig. 17), we expect significantly higher equivalence ratios at the start of low-temperature heat release. However, due to the extended delay before the rapid, high-temperature heat release begins, the equivalence ratio at SOC is not significantly higher than that seen for case 'A'.

The 10-50% burn time for case 'B' is approximately 25% longer than that of case 'A' (Fig. 23). Based on this factor alone, we might expect a greater degree of additional mixing along the premixed burn segment path than we see for case 'A'. However, due to the longer ignition delay associated with the lower O_2 concentration (despite similar ambient temperature), we anticipate that the energy of the injection event has dissipated to a greater extent and mixing rates are lower during this period for case 'B'. This factor counteracts the potential benefits of the increased ignition delay. Hence, we postulate that the premixed burn segments of the two combustion paths are nearly parallel.

Because the premixed burn period for path 'B' ends near TDC, at the end of the premixed burn path segment the temperature corresponds closely with the calculated maximum flame temperature. As further mixing occurs, the path follows the maximum flame temperature curve until volume expansion begins to drop the in-cylinder temperature. Note that, due to the low O_2 concentration, a relatively large volume of ambient fluid must be mixed with the partially-burned fuel to achieve an equivalence ratio of 1. Due to this factor, as well as the low flame temperatures and the proximity of the slow/rapid CO oxidation interface, it is likely to be more difficult to complete the mixing process before in-cylinder temperatures drop excessively for path 'B' than for path 'A'. This expectation is consistent with the earlier discussion of CO emissions, in which it was concluded that incomplete combustion of "under-mixed" fuel was likely the dominant source of CO emissions at high dilution levels.

SUMMARY AND CONCLUSIONS

Combustion performance and emissions were studied in an automotive high-speed, direct-injection, optically-accessible diesel engine over a broad range of charge dilution (EGR rate) and injection timing. Measurements of in-cylinder pressure and engine emissions, as well as images of combustion luminosity were obtained. The variation in cylinder pressure, apparent heat release rate, peak adiabatic flame temperature, NO_x emissions, soot luminosity, CO emissions, ignition delay, and burn times with dilution level and injection timing is presented and discussed, as well as the correlation of emissions, ignition delay, and burn times with adiabatic flame temperature. Additionally, the various factors influencing the fuel conversion efficiency are examined in detail. Finally, the above quantities, along with estimates of the equivalence ratio at ignition, are employed to clarify the effects of dilution level and injection timing on the path of the combustion process in the ϕ-T plane. Specific, major findings are summarized as follows:

- At fixed SOI, charge dilution decreases the adiabatic flame temperature due to the additional heat capacity of the diluent molecules. However, the earlier injection timing afforded by a dilute inlet charge can result in higher flame temperatures than seen with less dilution and later injection.
- NO_x and CO emissions, in addition to soot luminosity, correlate well with peak adiabatic flame temperature. NO_x emissions and soot luminosity increase with increasing flame temperature, while high flame temperatures reduce CO emissions due to rapid oxidation. The correlation of NO_x emissions with flame temperature is also found to be sensitive to the method of estimating the peak flame temperature. At the highest dilution levels and most retarded injection timing, the NO_x-temperature correlation exhibited a lower activation energy, indicating a much reduced sensitivity to peak flame temperature.

- The correlation of ignition delay with temperature and pressure closely follows expressions found in the literature. An inverse correlation with O_2 concentration is also observed.
- Images of natural combustion luminosity exhibit no soot luminosity until late in the pre-mixed burn period. The overall soot luminosity is decreased and becomes more uniform with increasing dilution.
- The equivalence ratio at ignition is not reduced as O_2 concentration is decreased (EGR rate increased). Although longer ignition delays are observed, a greater quantity of ambient fluid must be mixed with the fuel to achieve the same fuel/O_2 ratio. Consequently, a mixing-controlled combustion phase remains important under highly dilute operating conditions.
- The fuel conversion efficiency exhibits a maximum at moderate charge dilution levels and slightly retarded injection timing. The maximum fuel conversion efficiency is caused by a trade-off between combustion efficiency, work conversion efficiency, and heat losses.
- The postulated path of the combustion process in the ϕ-T plane clearly shows the benefits of dilution in avoiding soot and NO_x formation regions. However, mixing remains important if high fuel efficiency and low CO emissions are to be achieved.

ACKNOWLEDGMENTS

Support for this research was provided by the U.S. Department of Energy, Office of FreedomCAR and Vehicle Technologies. The research was performed at the Combustion Research Facility, Sandia National Laboratories, Livermore, California. Sandia is a multiprogram laboratory operated by Sandia Corporation, a Lockheed Martin Company, for the United States Department of Energy's National Nuclear Security Administration under contract DE-AC04-94AL85000. The NRL and Future Vehicle Technology Development Corps. of Korea supported Sanghoon Kook's visiting research. The authors express their appreciation to Mark Musculus and Cherian Idicheria for providing the high speed camera used in the experiments as well as Matlab source code for image processing and adiabatic flame temperature calculation. . Thanks are also due to Feng Tao of the University of Wisconsin (Madison) for his assistance in validating the estimated peak core gas temperatures.

REFERENCES

1. H. Akagawa, T. Miyamoto, A. Harada, S. Sasaki, N. Shimazaki, T. Hashizume, and K. Tsujimura, "Approaches to Solve Problems of the Premixed Lean Diesel Combustion", SAE Paper 1999-01-0183, 1999.
2. B. Walter, and B. Gaterllier, "Development of the High Power NADI^{TM} Concept Using Dual Mode Diesel Combustion to Achieve Zero NO_x and Particulate Emissions" SAE Paper 2002-01-1744, 2002.
3. S. L. Plee, T. Ahmad, and J. P. Myers, "Flame Temperature Correlation for the Effects of Exhaust Gas Recirculation on Diesel Particulate and NO_x Emissions", SAE Paper 811195, 1981.
4. N. Ladomatos, S. M. Abdelhalim, H. Zhao, and Z. Hu, "The Dilution, Chemical, and Thermal Effects of Exhaust Gas Recirculation on Diesel Engine Emissions – Part 1: Effect of Reducing Inlet Charge Oxygen", SAE Paper 961165, 1996.
5. M. P. B. Musculus, "On the Correlation between NO_x Emissions and Diesel Premixed Burn", SAE Paper 2004-01-1401, 2004.
6. K. Akihama, Y. Takatori, K. Inagaki, S. Sasaki, and A. M. Dean, "Mechanism of the Smokeless Rich Diesel Combustion by Reducing Temperature", SAE Paper 2001-01-0655, 2001.
7. T. Kamimoto and M. H. Bae, "High Temperature for the Reduction of Particulate in Diesel Engines", SAE Paper 880423, 1988.
8. T. Kitamura, T. Ito, J. Senda, and H. Fujimoto, "Mechanism of Smokeless Diesel Combustion with Oxygenated Fuels Based on the Dependency of the Equivalence Ratio and Temperature on Soot Particle Formation", International Journal of Engine Research, Vol. 3, No. 4, pp.223-247, 2002
9. L. M. Pickett and D. L. Siebers, "Non-sooting, low flame temperature mixing-controlled DI diesel combustion", SAE Paper 2004-01-1399, 2004.
10. P. C. Miles, D. Choi, L. M. Pickett, I. P. Singh, N. Henein, B. A. RempelEwert, H. Yun and R. D. Reitz, "Rate-Limiting Processes in Late-Injection, Low-Temperature Diesel Combustion Regimes", Proc. of THIESEL Conference on Thermo- and Fluid Dynamic Processes in Diesel Engines, Sep. 8-10, Valencia, Spain, 2004.
11. S. Kimura, Y. Matsui, and Y. Enomoto, "An Experimental Analysis of Low-Temperature and Premixed Combustion for Simultaneous Reduction of NOx and Particulate Emissions in Direct Injection Diesel Engines", International Journal of Engine Research, Vol. 3, No. 4, pp.249-259, 2002
12. M. Weißbäck, J. Csató, M. Glensvig, T. Sams, and P. Herzog, "Alternative Combustion – An Approach for Future HSDI Diesel Engines", MTZ Worldwide, Vol. 64, No. 9, pp.17-20, 2003
13. R. M. Wagner, J. B. Green Jr., T. Q. Dam, K. D. Edwards, and J. M. Storey, "Simultaneous Low Engine-Out NO_x and Particulate Matter with Highly Diluted Diesel Combustion", SAE Paper 2003-01-0262, 2003.
14. C. J. Mueller and G. C. Martin, "Effect of Oxygenated Compounds on Combustion and Soot Evolution in a DI Diesel Engine: Broadband Natural Luminosity Imaging", SAE Paper 2002-01-1631, 2002.
15. W. C. Reynolds, "The Element Potential Method for Equilibrium Analysis: Implementation of the Interactive Program Stanjan", Department of Mechanical Engineering, Stanford University, 1986.

16. C. T. Bowman, “Kinetics of Pollutant Formation and Destruction in Combustion”, Prog. Energy Combust. Sci., Vol. 1, pp.33-45, Pergamon Press, 1975.
17. J. E. Dec, “A Conceptual Model of DI Diesel Combustion Based on Laser-Sheet Imaging”, SAE Paper 970873, 1997
18. R. Egnell, “The Influence of EGR on Heat Release Rate and NO Formation in a DI Diesel Engine”, SAE 2000-01-1807, 2000
19. D.A. Kouremenos, D.T. Hountalas and .B. Binder, “The Effect of EGR on the Performance and Pollutant missions of Heavy Duty Diesel Engines Using Constant and Variable AFR”, SAE Paper 2001-01-0198, 2001
20. C. J. Mueller, W. J. Pitz, L. M. Pickett, G. C. Martin, D. L. Siebers, and C. K. Westbrook, “Effects of Oxygenates on Soot Processes in DI Diesel Engines: Experiments and Numerical Simulations”, SAE Paper 2003-01-1791, 2003.
21. P. Adomeit, S. Pischinger, M. Becker, H. Rohs and A. Greis, “Laser Optical Diagnostics and Numerical Analysis of HDSI Combustion”, THIESEL 2004 Conference on Thermo- and Fluid Dynamic Processes in Diesel Engines, Sep. 8-10, Valencia, Spain, 2004.
22. M. Sjöberg, J. E. Dec, “An investigation into lowest acceptable combustion temperature for hydrocarbon fuels in HCCI engines”, Proceedings of the Combustion Institute, Vol. 30, pp.2719-2726, 2005
23. T. Minagawa, H. Kosaka and T. Kamimoto, “A study on Ignition Delay of Diesel Fuel Spray via Numerical Simulation”, SAE Paper 2000-01-1892, 2000.
24. J. B. Heywood, “Internal Combustion Engine Fundamentals”, International Edition, McGraw-Hill, Inc., 1988.
25. D. Siebers, B. Higgins, and L. Pickett, “Flame Lift-Off on Direct-Injection Diesel Fuel Jets: Oxygen Concentration Effect”, SAE Paper 2002-01-0890, 2002.
26. P. F. Flynn, R. P. Durrett, G. L. Hunter, A. O. zur Loye, O. C. Akinyemi, J. E. Dec, and C. K. Westbrook, “Diesel Combustion: An Integrated View Combining Laser Diagnostics, Chemical Kinetics, And Empirical Validation”, SAE Paper 1999-01-0509, 1999

NOMENCLATURE

ASOI	After Start Of Injection
ATDC	After Top Dead Center
CAD	Crank Angle Degrees
DCCS	Dilution Controlled Combustion System
EGR	Exhaust Gas Recirculation
HCCI	Homogeneous Charge Compression Ignition
HCLI	Homogeneous Charge Late Injection
HPLI	Highly Premixed Late Injection
IMEP	Indicated Mean Effective Pressure
MK	Modulated Kinetics
NO_x	Nitrogen Oxides (NO and NO_2)
SOC	Start of Combustion (10 % heat release)
SOI	Start of Injection
X_{O_2}	Intake O_2 Mole Fraction
X_{N_2}	Intake N_2 Mole Fraction
$\dot{m}_f$	Measured Fueling Rate
ϕ	Equivalence Ratio
$\overline{p}_a$	Average Ambient Pressure
τ_{id}	Ignition delay from SOI to SOC
T_f	Adiabatic Flame Temperature at Stoichiometry
$\overline{T}_a$	Average Ambient Temperature

CONTACT

Sanghoon Kook, kooks@kaist.edu